Status Report No. 1

University of Maryland, College Park
Department of Aerospace Engineering

A Study of the Drooped Leading Edge Airfoil

John D. Anderson, Jr. and Jewel B. Barlow

Department of Aerospace Engineering

NASA
Langley Research Center
Daniel Dicarlo, Mail Stop 247
Hampton, VA 23655

NASA Grant No. 1570

April, 1979

A Study of the Drooped Leading Edge Airfoil

Introduction

This report reviews progress to date on a study of the drooped leading-edge airfoil. As noted in previous reports (ref. 1, 2 and 3), the use of a drooped leading edge airfoil reduces the tendency for an airplane to enter a spin after stall occurs. The drooped airfoil consists of a baseline airfoil on which an abrupt change of airfoil cross-section is made at about midspan from the fuselage. The outboard portion of the wing has a cross-section in which the airfoil is nearly flat bottom and the leading edge is "drooped" downward relative to the inboard baseline wing.

Wind tunnel tests are currently underway at the University of Maryland to look at various aspects of the drooped-leading edge airfoil. Parametric studies are being made to look at the effects of relative chord and the effects of relative droop (see Fig. 1). In the relative chord tests, a 12.7 cm chord baseline wing (NACA 0015) will be fitted with a "glove" to extend the leading edge on 50% of the wing span. These tests are aimed at determining the effects of chord extension. In the relative "droop" tests, the glove will be shaped to produce a variation in the droop of the leading edge.

The following section gives a brief description of the test facilities and the models currently being used.

1. Kroeger, R. A. and Feistel, T. W., "Reduction of Stall-Spin Entry Tendencies Through Wing Aerodynamic Design," SAE Paper 760481, April 1976.
2. Feistel, T. W. and Anderson, S. B., "A Method for Localizing Wing Flow Separation at Stall to Alleviate Spin Entry Tendencies," AIAA Paper 78-1476, 1978.
3. Aviation Week, Sept. 11, 1978, pp. 103, 105.

Experimental Program

Two series of tests have been completed: 1) tests of two-dimensional baseline models spanning the working section of the Aerospace Boundary Layer Research Tunnel (see Fig. 3) and 2.) tests of a three-dimensional reflection-plane model in the Glenn L. Martin Subsonic Wind Tunnel Facility (see Fig. 4).

Three baseline models were used for the 2-D tests: NACA 0015, 0014.6 and 0014.2 (see Fig. 2 and 3). The 14.6% and 14.2% models were derived from NACA 0015 sections by increasing the chord and matching the profiles in the aft section. These tests were performed to obtain reference data on each baseline configuration before the models are joined together as shown in Fig. 1. Force balance data (lift, drag, pitching moment) were obtained for each model at a free-stream Reynold's number of 2.66×10^6/m. In addition, oil flow visualization tests were performed at various angles of attack.

A second series of tests were completed in the Glenn L. Martin Tunnel using an existing NACA 64_1A211 airfoil (see Fig. 4). The leading edge flap was segmented in three parts which allowed various baseline/drooped leading edge configurations to be tested. Force balance and flow visualization tests were completed at chord Reynolds numbers of 0.44×10^6, 1.4×10^6 and 2.11×10^6.

Experimental Results

A. Tests of NACA 0015, 0014.6 and 0014.2 Airfoils

1. oil flow

A series of photographs of oil flow tests on the three baseline wings is presented in Figs. 5 - 12. For all three models at an angle of attack of $\alpha = 0^{o}$, a separated flow region existed on the top and bottom from .50C to about 0.70C (Fig. 5). This laminar separation bubble was observed to move forward on the leeward side and rearward on the windward side as α was increased. As the wings neared the stall point, the flow over the central portion was reversed with vortex patterns occurring to each side (e.g. Fig. 11).

In the next set of tests, grit (0.023 cm.) was placed on a narrow strip at the 5% chord location. Although this eliminated the apparent laminar separation bubble at $\alpha = 0^{o}$, the oil flow patterns at angle of attack were essentially unchanged.

2. force balance

Force balance measurements were made on all three wings to obtain lift, drag and pitching moment data. Some of the results of these tests are shown in Figs. 13 - 16. The life curve slope for all three models is the same for tests without grit (Fig. 13). The use of grit appears to reduce the lift curve slope for the models tested here (Fig. 14 and 15). In addition, the wings with grit were observed to stall at a lower angle of attack. The use of grit also increased $C_{D_{min}}$ by 100% (Fig. 16).

B. Test of NACA 64_1A211 Wing

1. flow visualization

Flourescent oil flow tests were completed on the following configurations (see Fig. 4)

Configuration 1 - baseline wing with no leading edge deflection

Configuration 2 - entire leading edge deflected at 20°

Configuration 3 - segment N_1 undeflected N_2 and N_3 deflected 10°

Configuration 4 - segment N_1 undeflected N_2 and N_3 deflected 20°

Configuration 5 - segments N_1 and N_2 undeflected N_3 deflected 20°

Configuration 6 - segments N_2 and N_3 undeflected N_1 deflected 20°

Photographs of the oil flow patterns observed on these models are presented in Figs. 17 - 31. For all of the configurations tested at $\alpha = 0^\circ$, the flow was fully attached and uneffected by the drooped sections.

The most notable oil pattern observed on the baseline wing occurred in the vicinity of stall at $\alpha = 15^\circ$ (Fig. 18). A large swirl pattern is apparent at 70% span and mid-chord. A weaker vortex pattern rotating in the opposite sense is present near to the floor of the test section.

When a portion of the leading edge is deflected (drooped), a strong vortex pattern is apparent at about 55% span near to the trailing edge for $\alpha = 16^\circ$ (Figs. 21, 24, 27 and 30). It is of interest to note that this pattern occurs in the same general area for all of the drooped configurations tested here. At $\alpha = 30^\circ$, this vortex pattern appears to move toward mid-chord. The flow field over the outer span of the wing at $\alpha = 30^\circ$ is very complex as shown by the presence of a number of recirculatory regions (Figs. 22, 25 28 and 31).

2. force balance

Lift and drag data obtained on the NACA 64_1A211 airfoil are shown in Figs. 32 - 34. All configurations showed a very sharp drop in C_L at stall except for configuration 2 which had the entire leading edge drooped to 20°. The largest maximum lift coefficient $C_{L_{max}}$ occurred for configuration 6,

while the smallest $C_{L_{max}}$ occurred for configuration 1 (baseline wing). The largest $C_{D_{min}}$ occurred for configuration 2 (Fig. 34). As noted in Fig. 33, drooping sections of the leading edge helps to increase the lift coefficient in the post stall region. Drooping also increases the lift curve slope in the pre-stall region (Fig. 33).

Future Test Plans

1. Tests on NACA Section 0015 in the large tunnel, with and without the leading-edge gloves. These tests will comprise of:

   a. force tests

   b. pressure measurements

   c. flow visualization tests

2. Force and flow visualization tests on NACA Section 64_1A211 in the large tunnel.

3. Parametric (force and flow visualization tests) studies of relative chord and relative droop in the boundary layer research tunnel (2-D and 3-D tests).

4. Flow field survey on one of the wings (configuration to be decided later) in the boundary layer research tunnel.

5. Possible pressure survey on one wing (configuration to be decided later) in the boundary layer research tunnel.

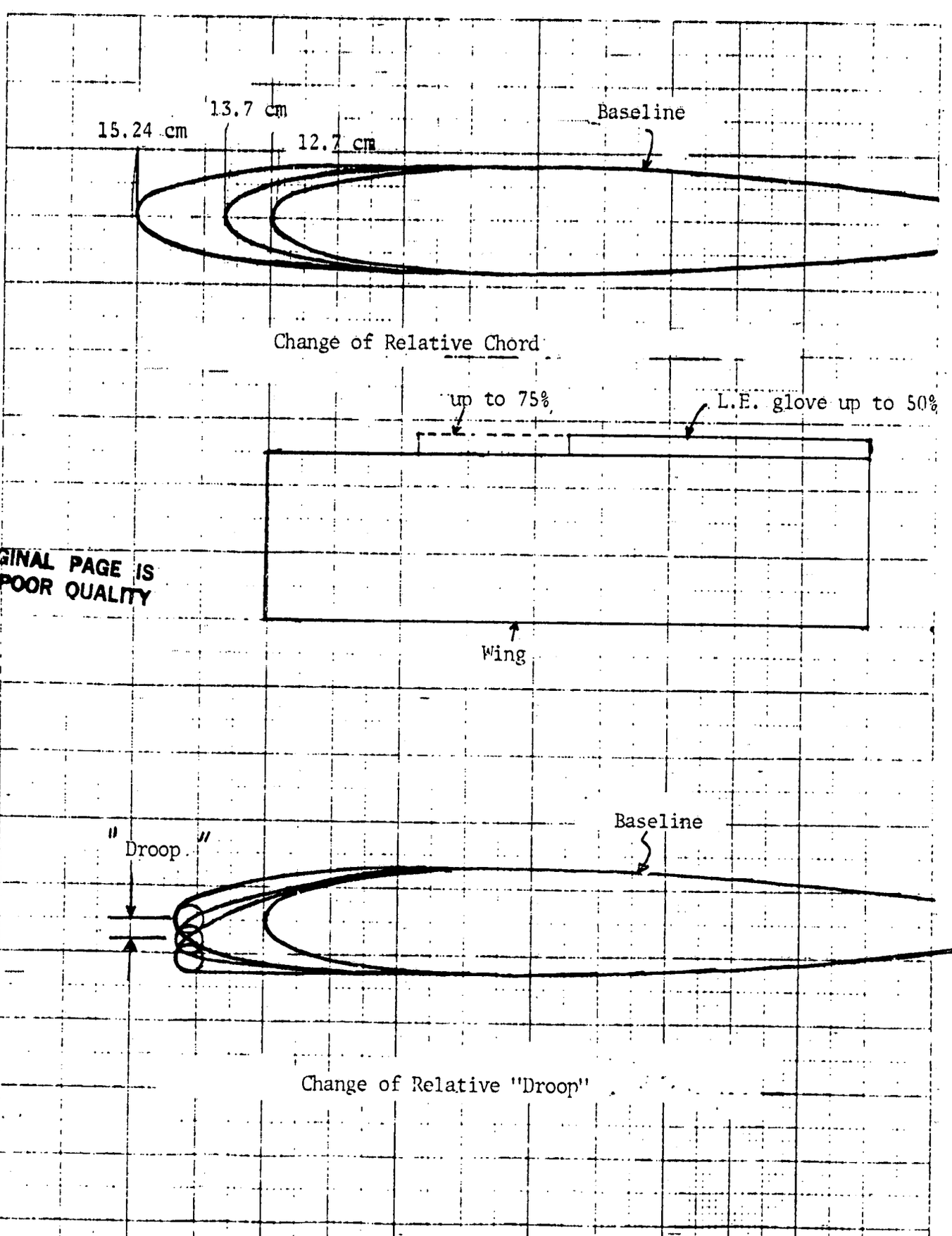

Fig. 1

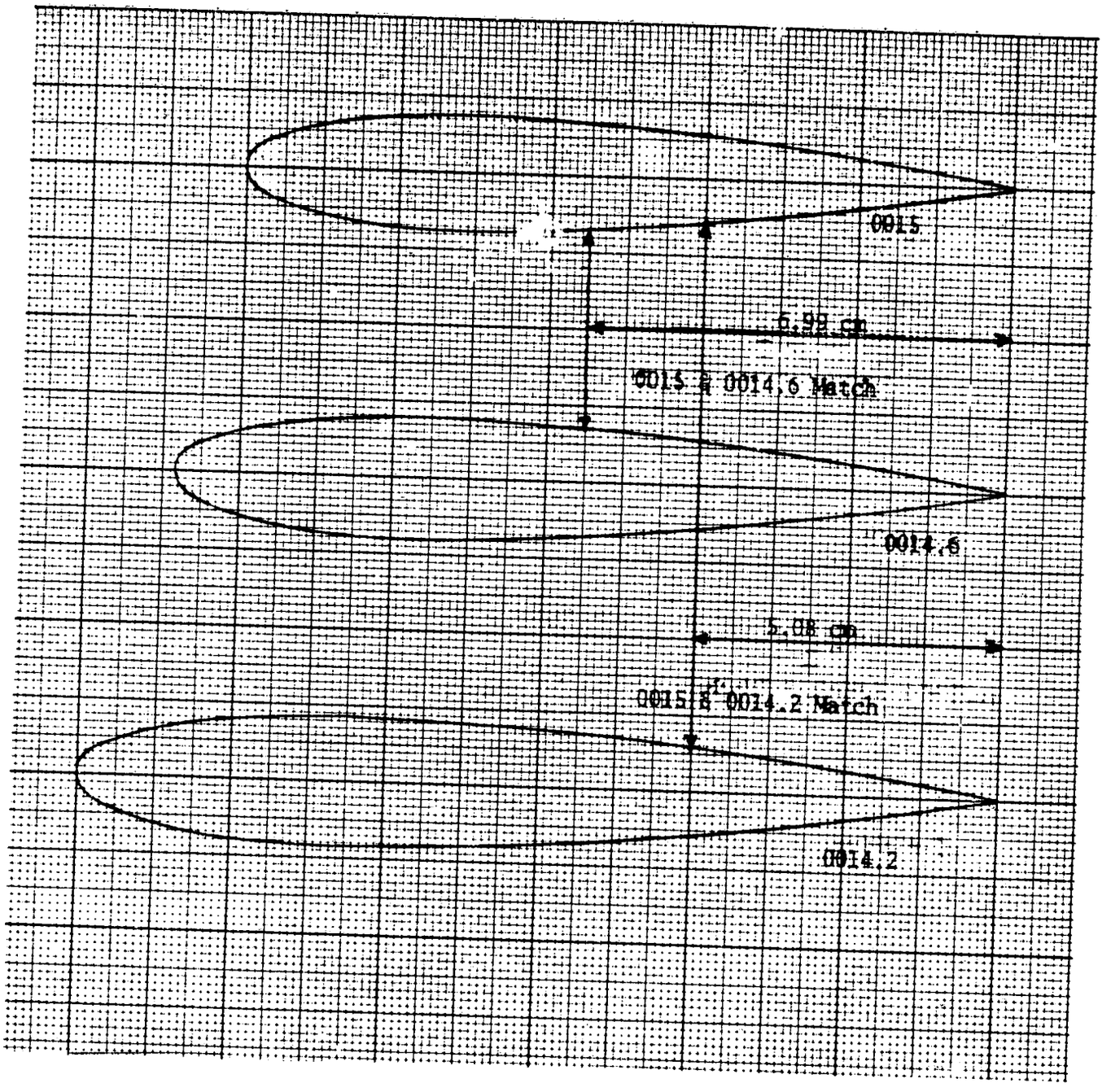

Fig. 2 -- Sketch of Airfoils, NACA-0015, 0014.6, 0014.2

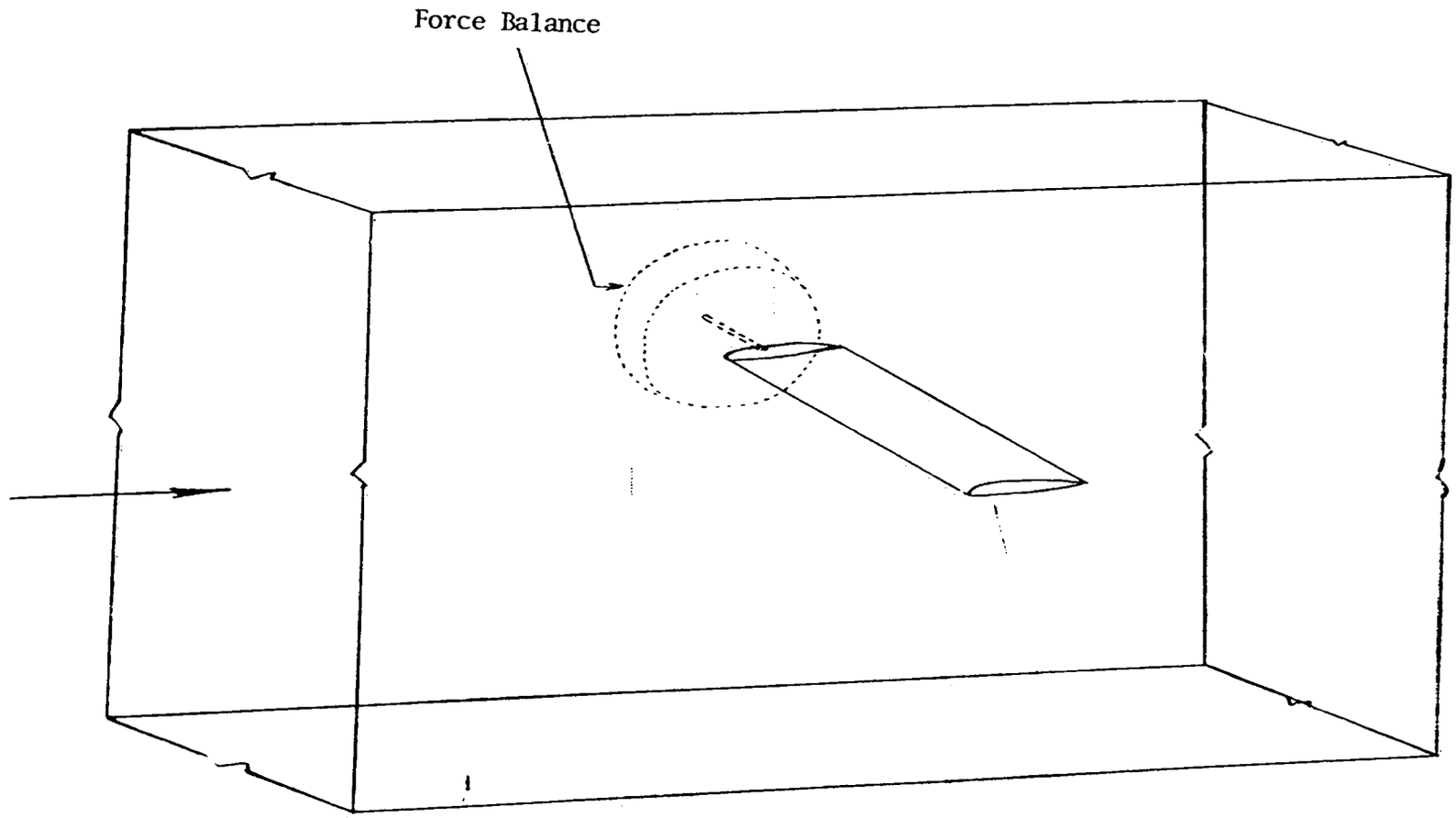

TEST SECTION

43.94 x 116.33 cm

Wing Model

NACA	Chord	Length
0015	12.7 cm	43.94 cm
0014.6	13.76 cm	43.94 cm
0014.2	15.24 cm	43.94 cm

Fig. 3 -- Sketch of 2-D Model in Boundary Layer Tunnel

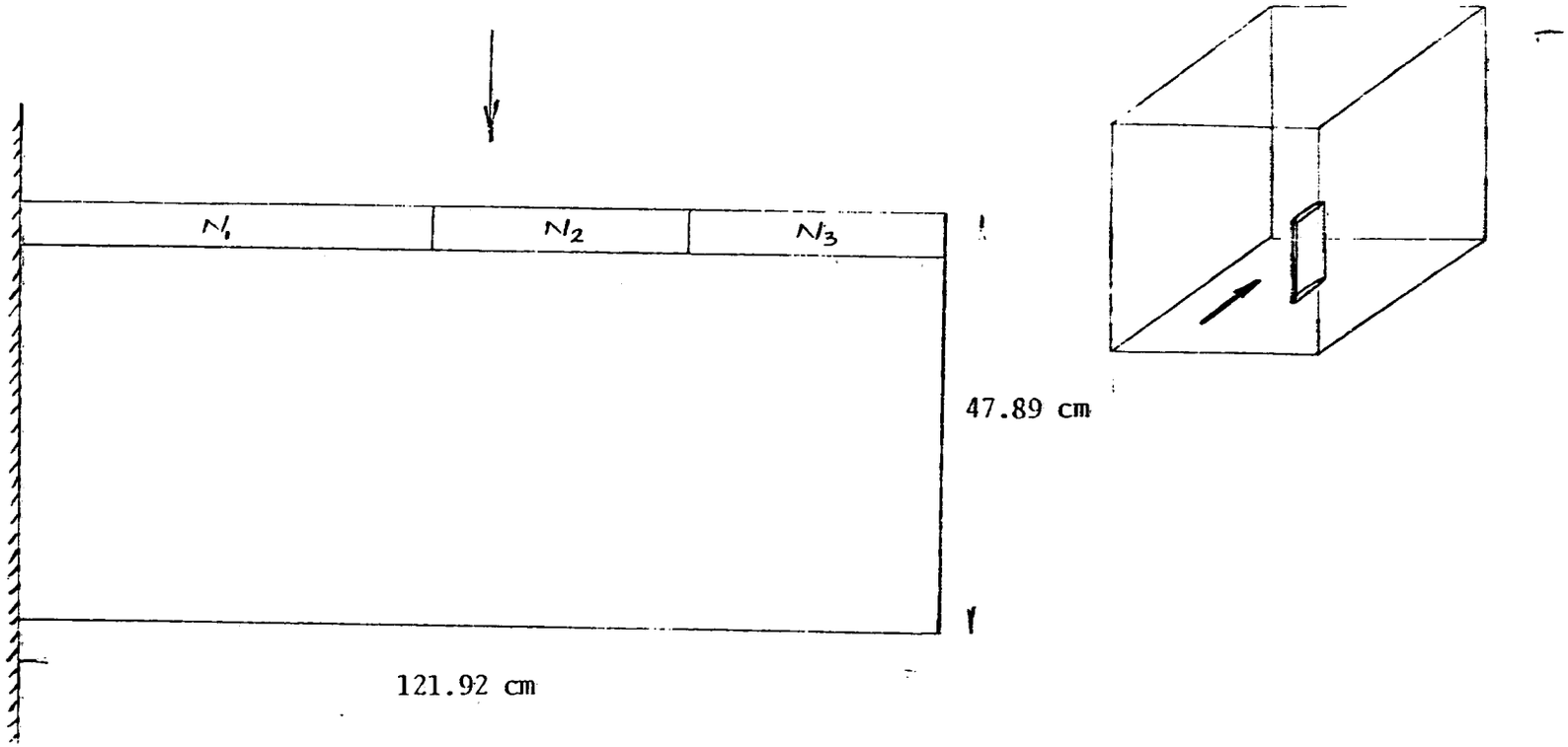

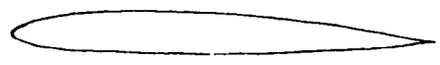

Section Without L.E. Droop

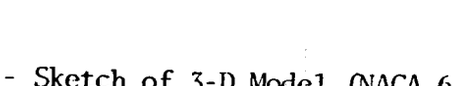

Section With Typical L.E. Droop A - Hing Point BC - Fairing

Fig. 4 -- Sketch of 3-D Model (NACA 64_1A211) and Location of Leading-Edge Flaps

Fig. 5 -- Oil Flow Pattern
0015, Top Surface, $\alpha = 0^{o}$

Fig. 6 -- Oil Flow Pattern

0015, Bottom Surface, $\alpha = 10^{o}$

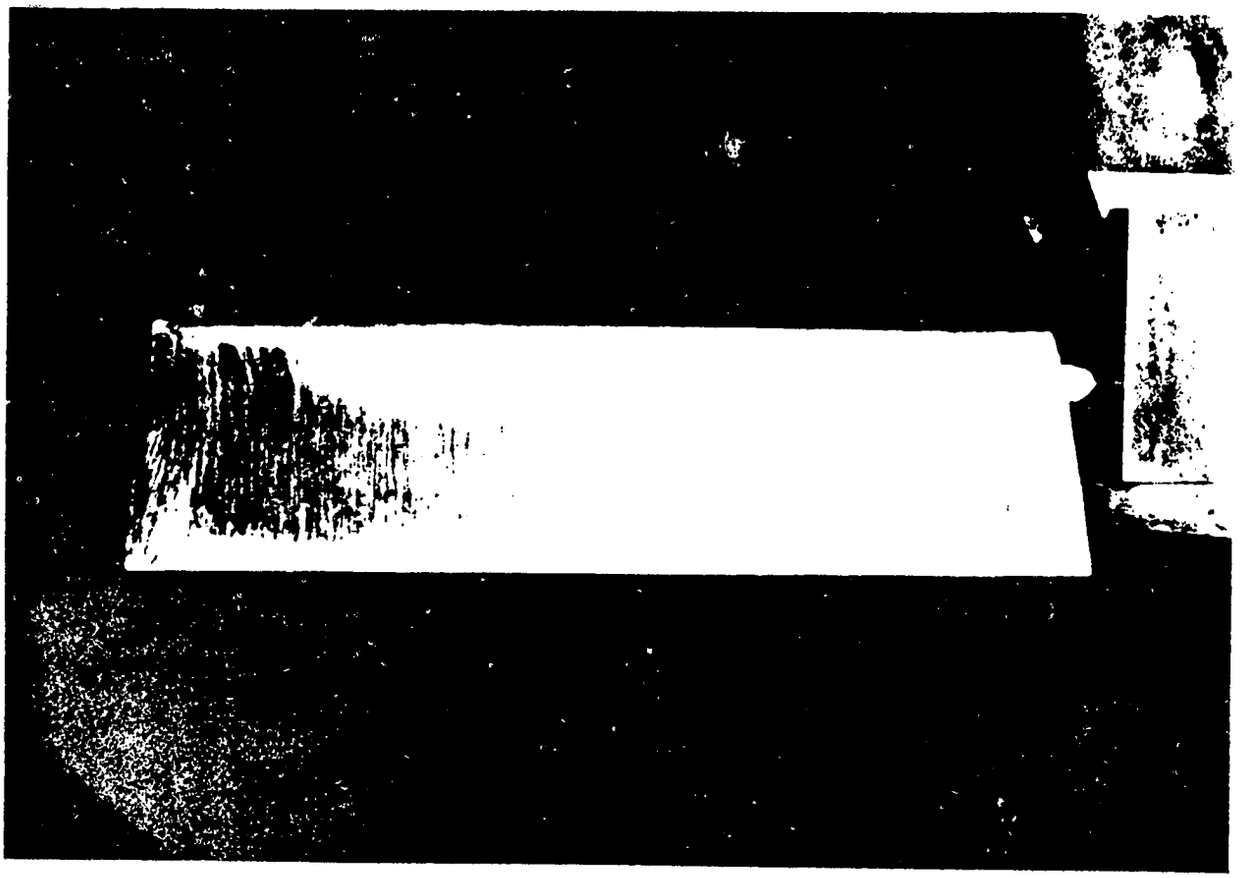

Fig. 7 -- Oil Flow Pattern

0014.6, Top Surface, $\alpha = 5^{o}$

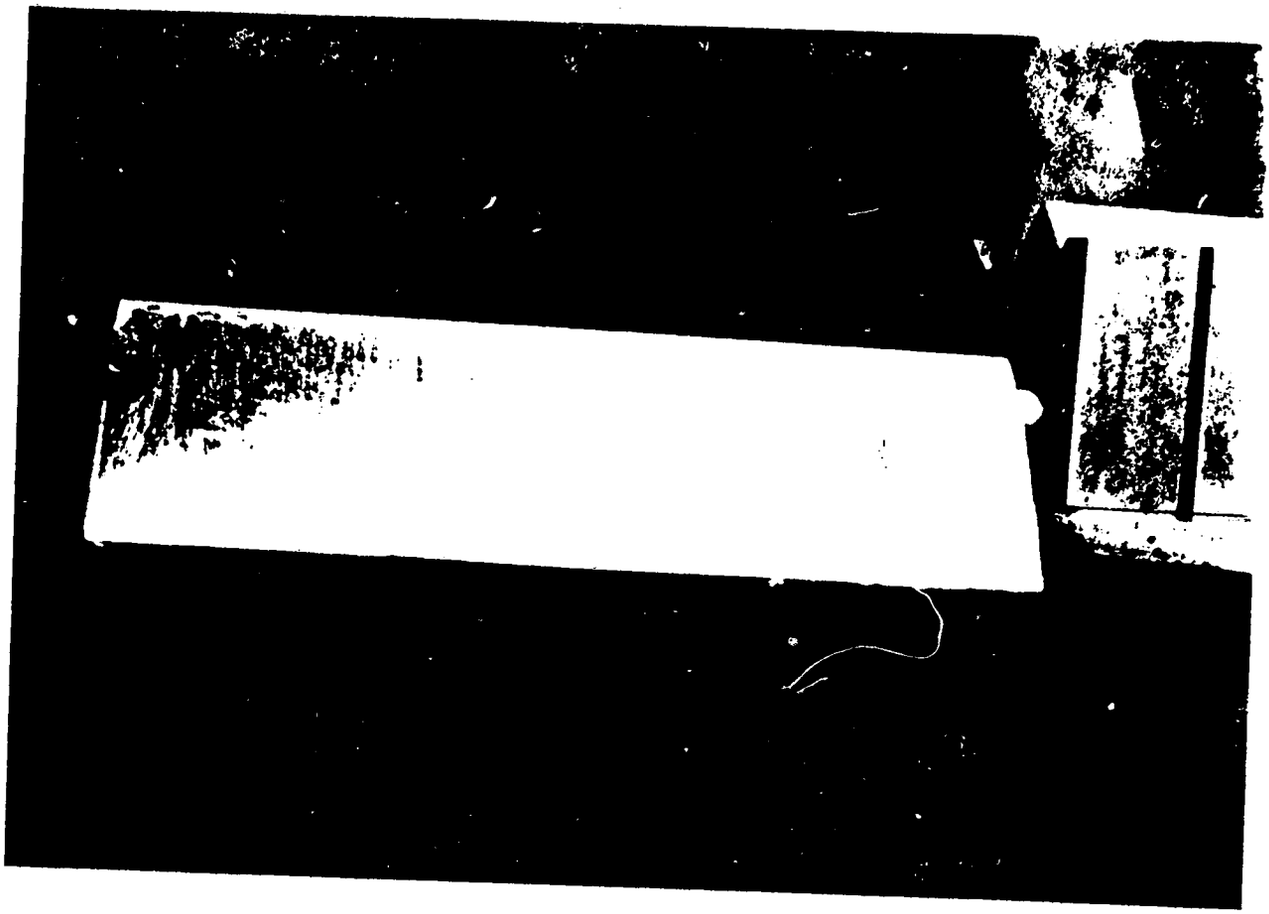

Fig. 8 -- Oil Flow Pattern

0014.6, Top Surface, $\alpha = 10^{o}$

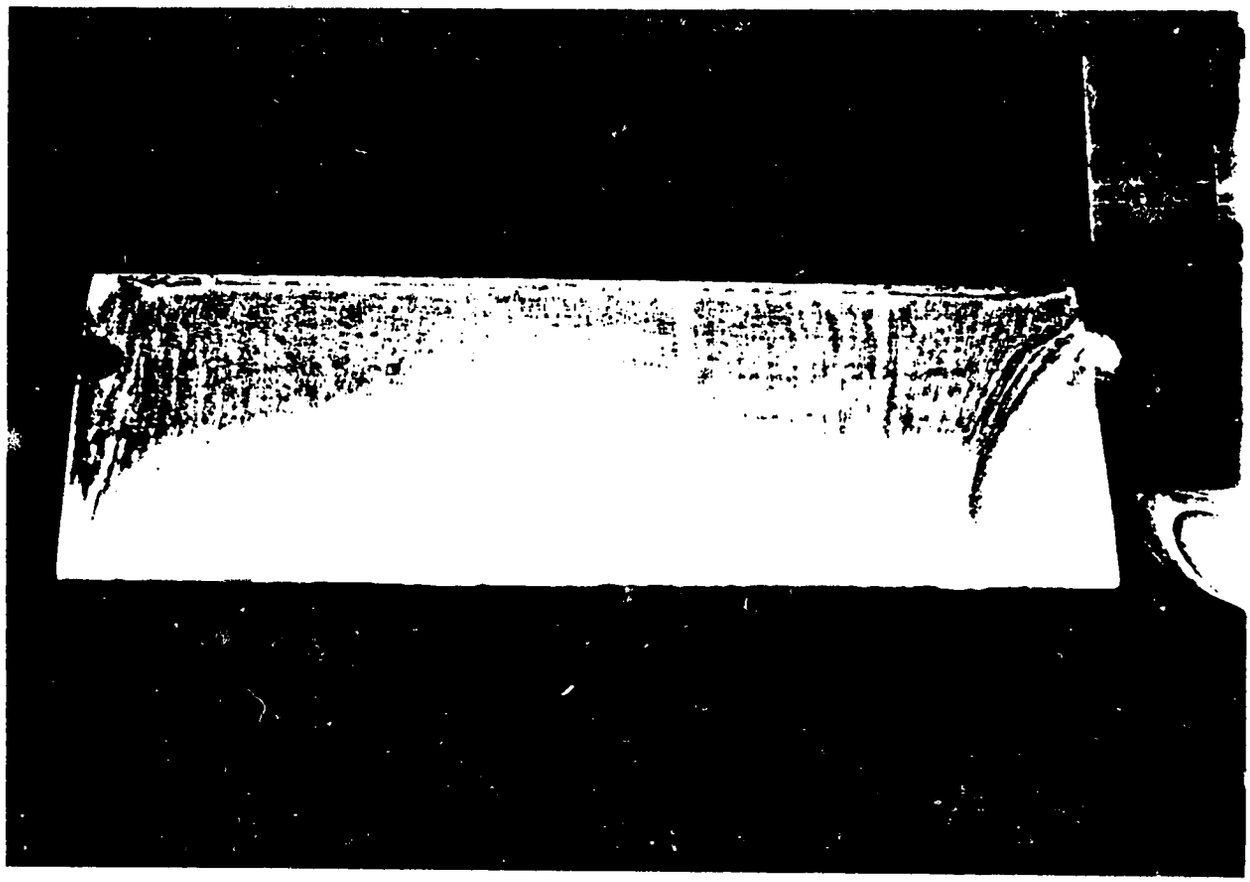

Fig. 9 -- Oil Flow Pattern

0014.2, Top Surface, $\alpha = 13^{o}$

Fig. 10 -- Oil Flow Pattern

0014.2, Bottom Surface, $\alpha = 13^{o}$

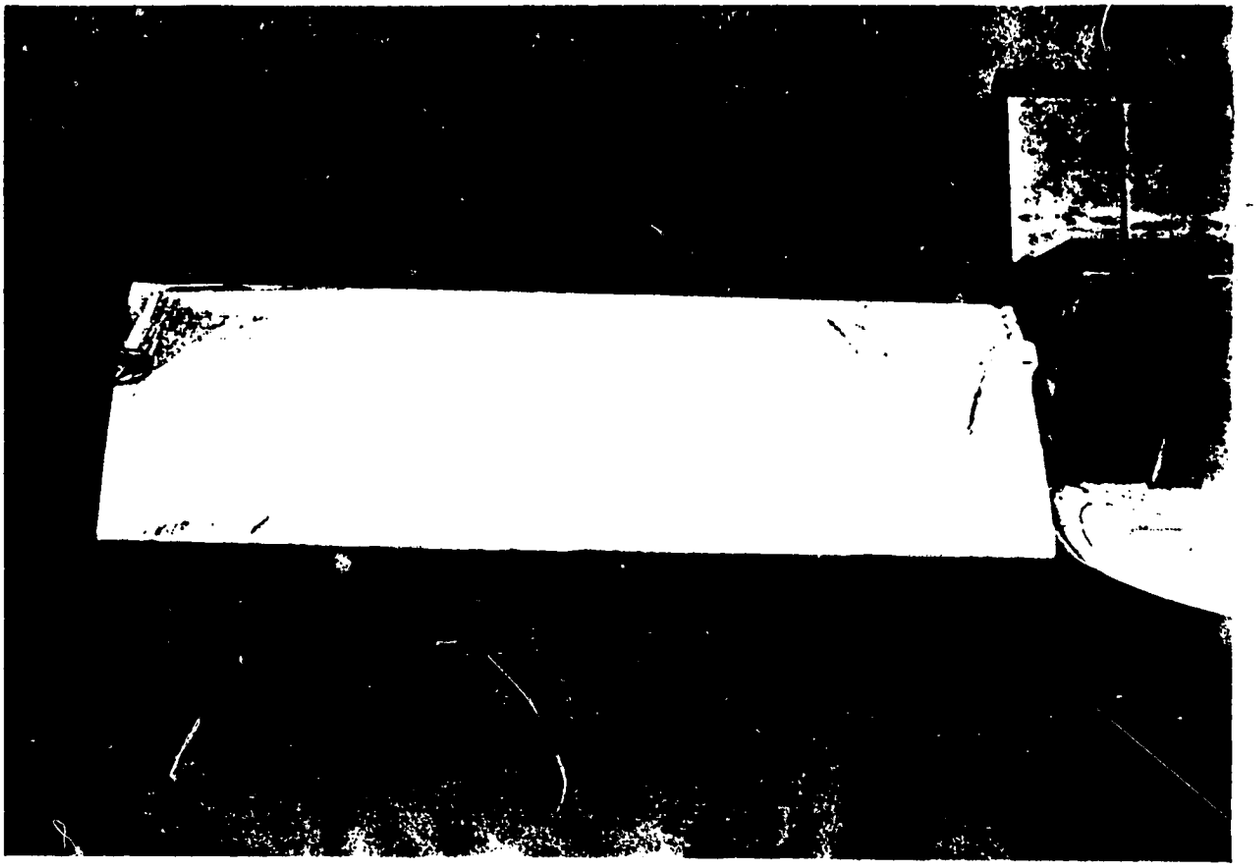

Fig. 11 -- Oil Flow Pattern

0014.2, Top Surface, $\alpha = 14^{o}$

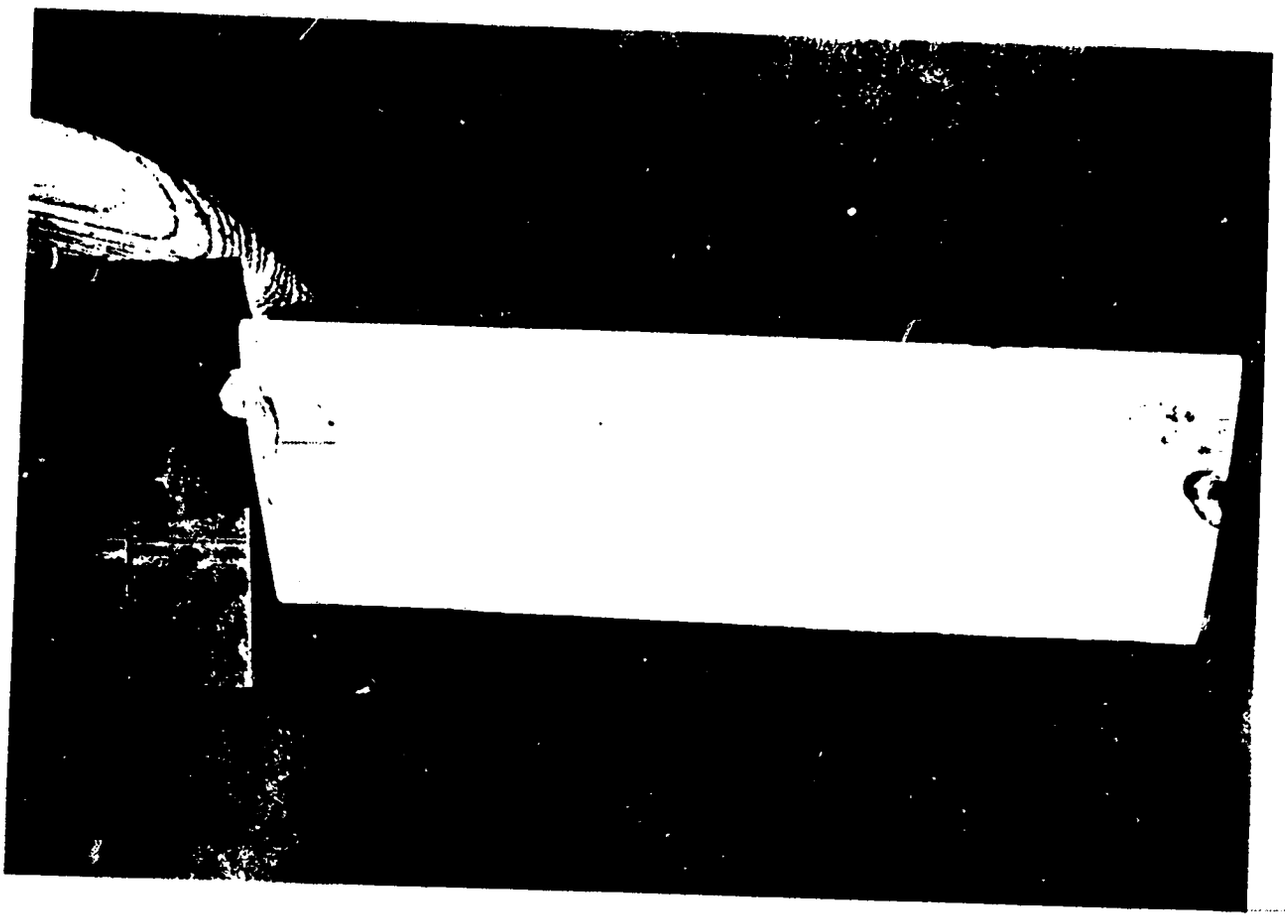

Fig. 12 -- Oil Flow Pattern

0014.2, Bottom Surface, $\alpha = 14^{o}$

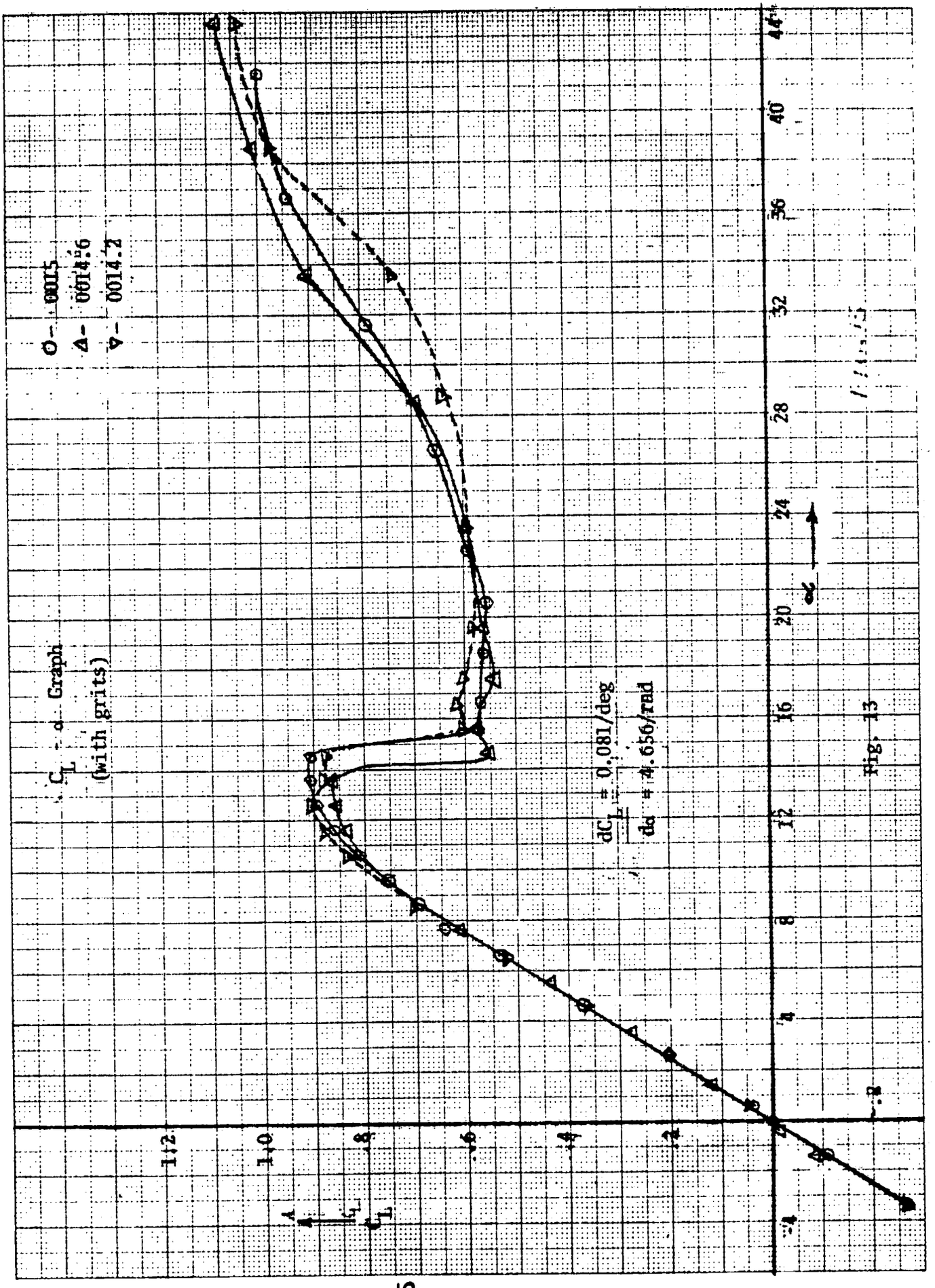

Fig. 13

10 Millimeters to the Centimeter

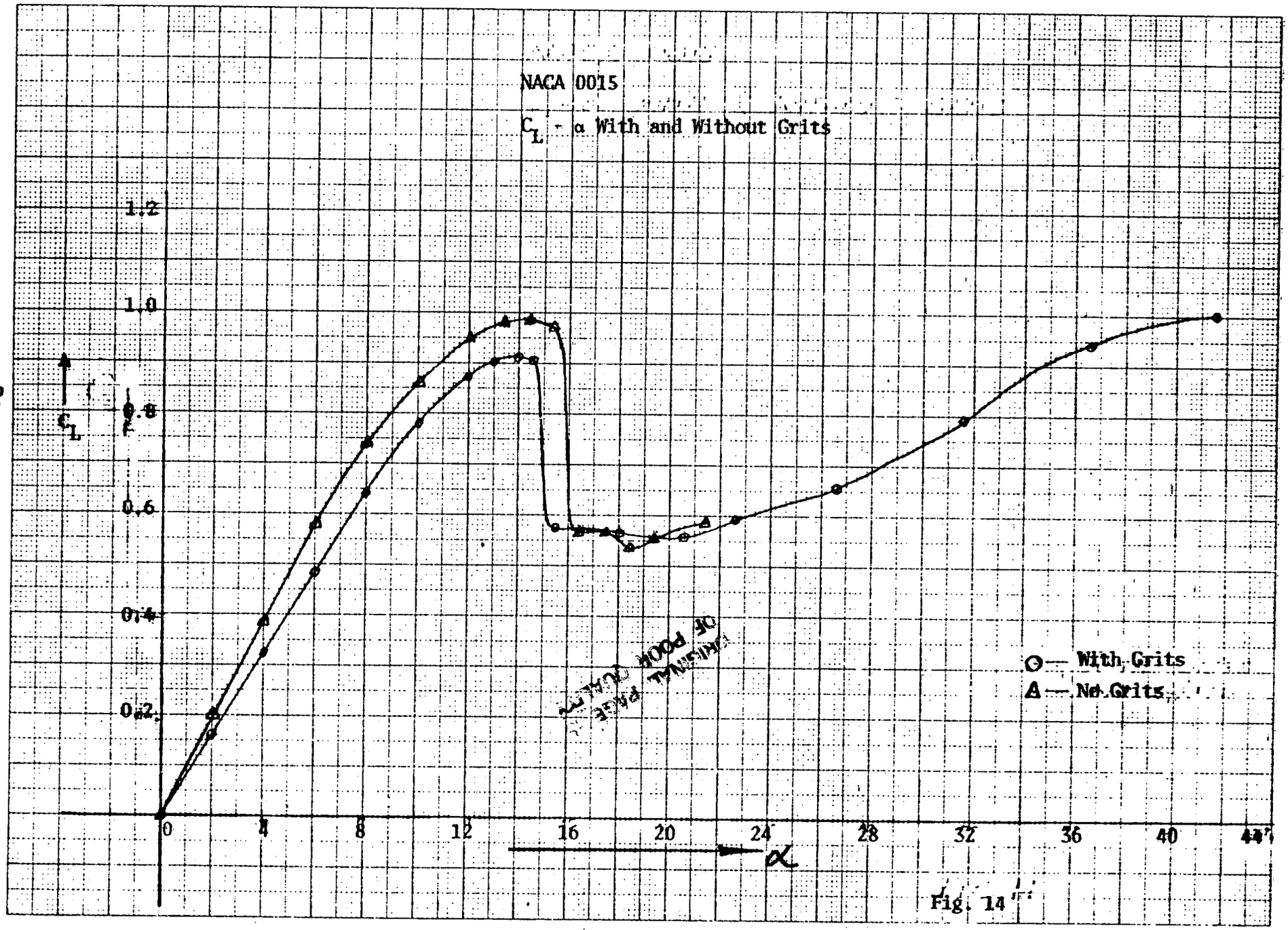

Fig. 14

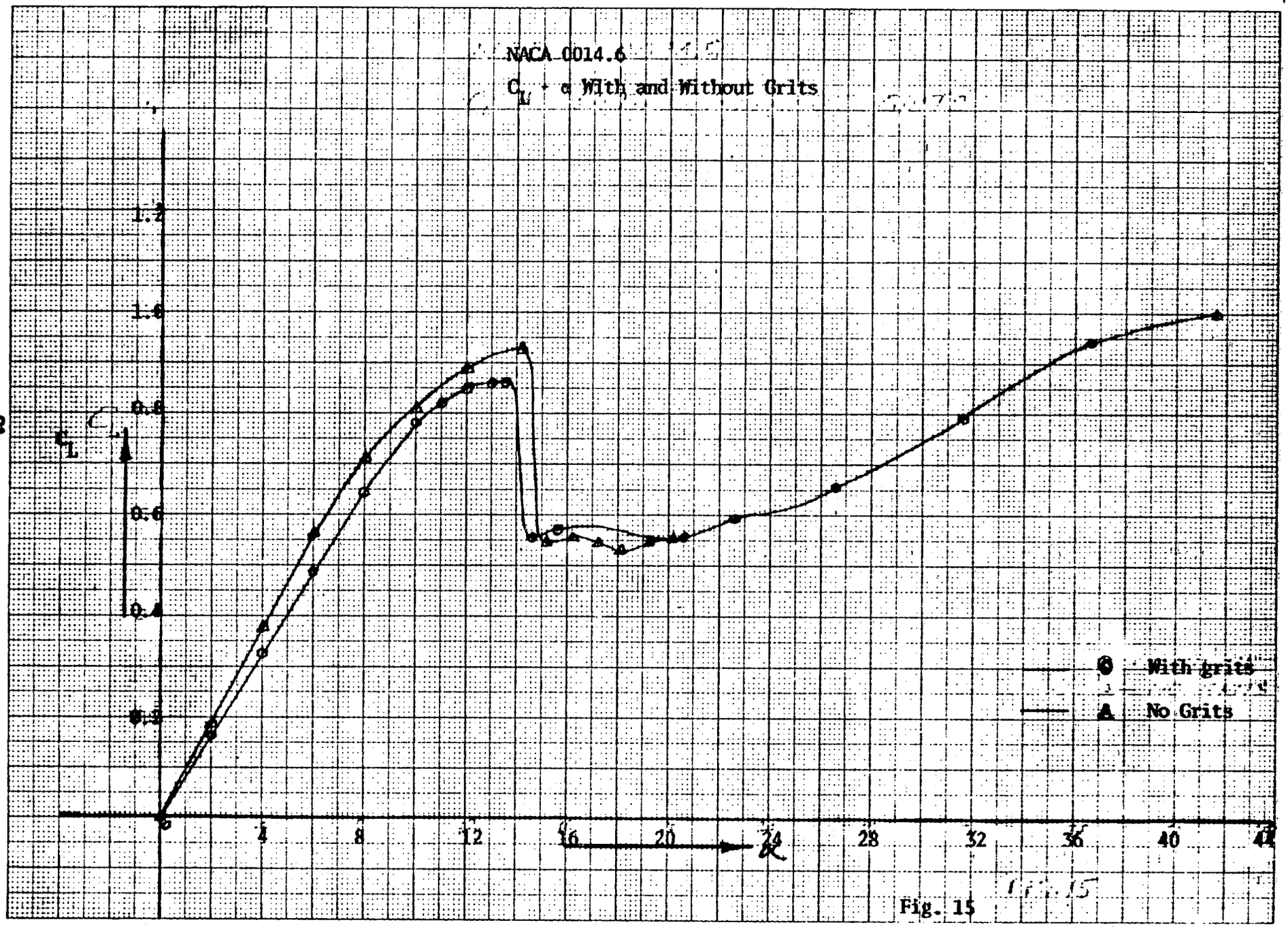

Fig. 15

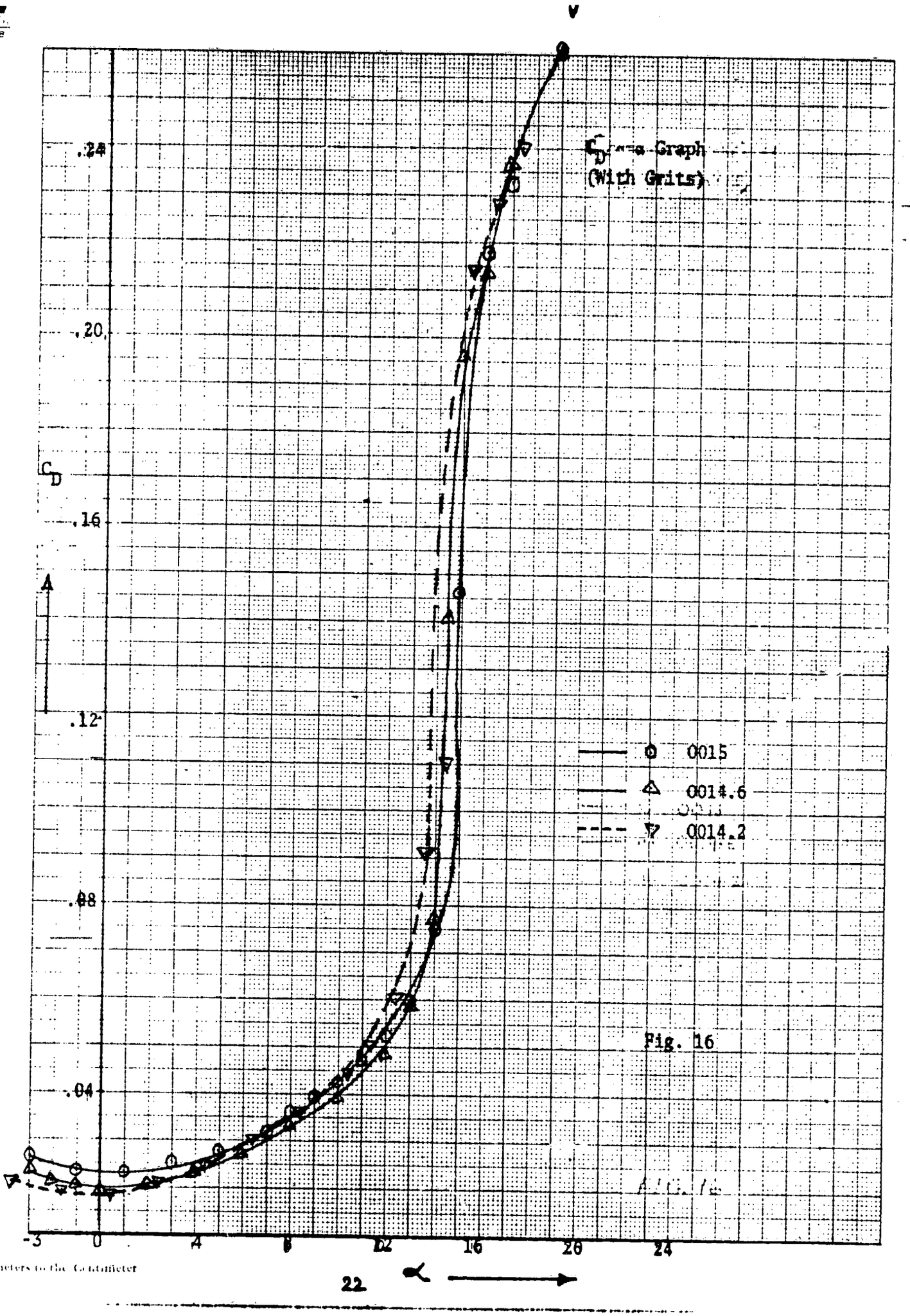
V
C_D vs α Graph
(With Grits)
.24
.20
C_D
.16
.12
.08
.04
0015
0014.6
0014.2
-3
0
4
8
12
16
20
24
α

Fig. 16

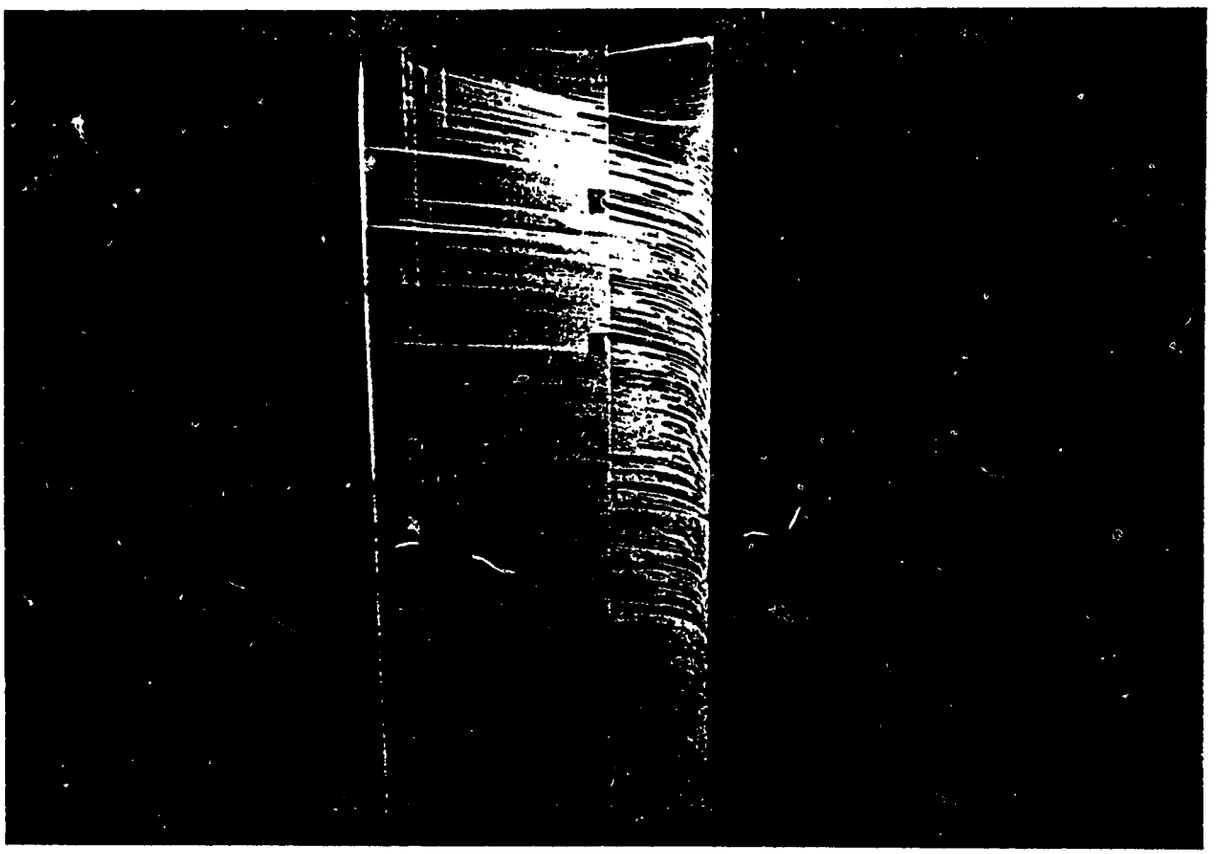

Fig. 17 -- Flow Pattern
NACA-64$_1$A211, Conf. - $N_1 = N_2 = N_3 = 0^o$
$V = 67.06$ m/s, $\alpha = 10^o$

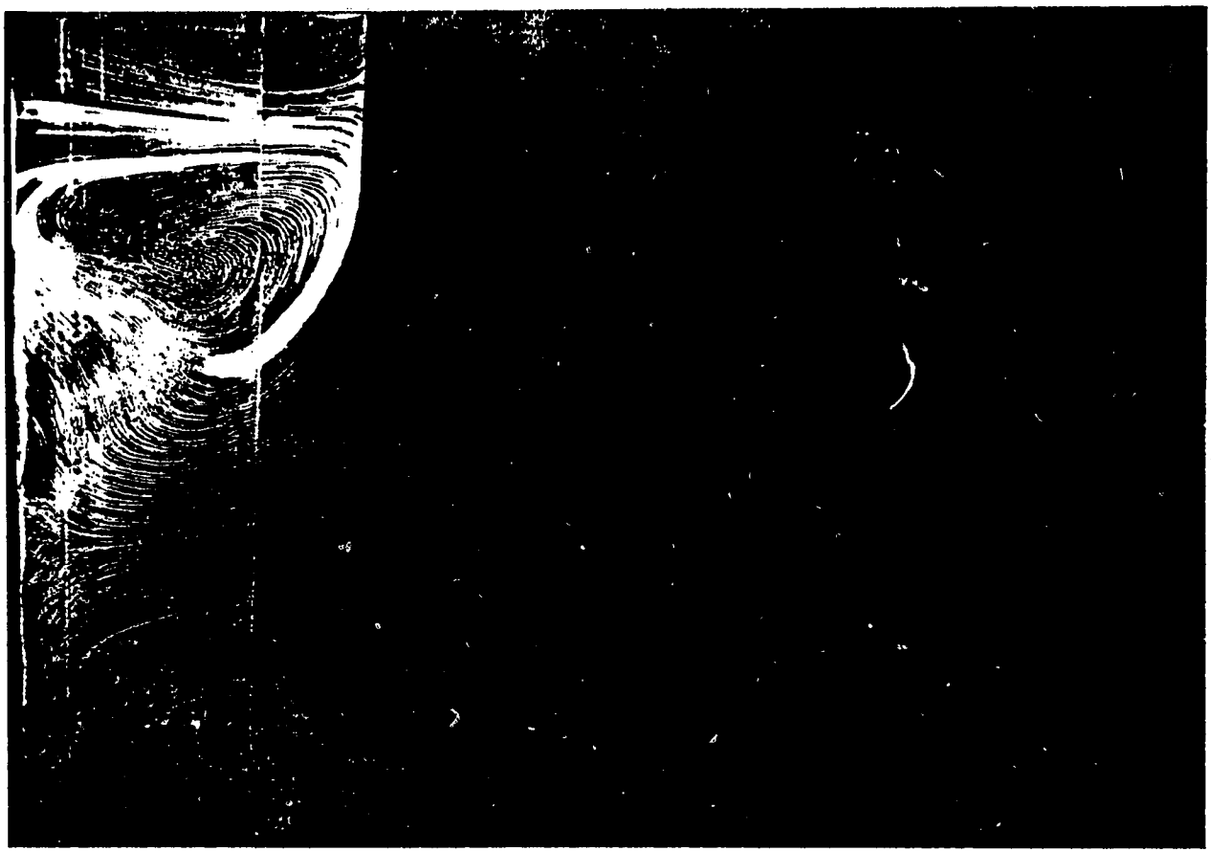

Fig. 18 - Flow Pattern
$NACA\text{-}64_1A211$, Conf. - $N_1 = N_2 = N_3 = 0^o$
$V = 67.06$ m/s, $\alpha = 15^o$

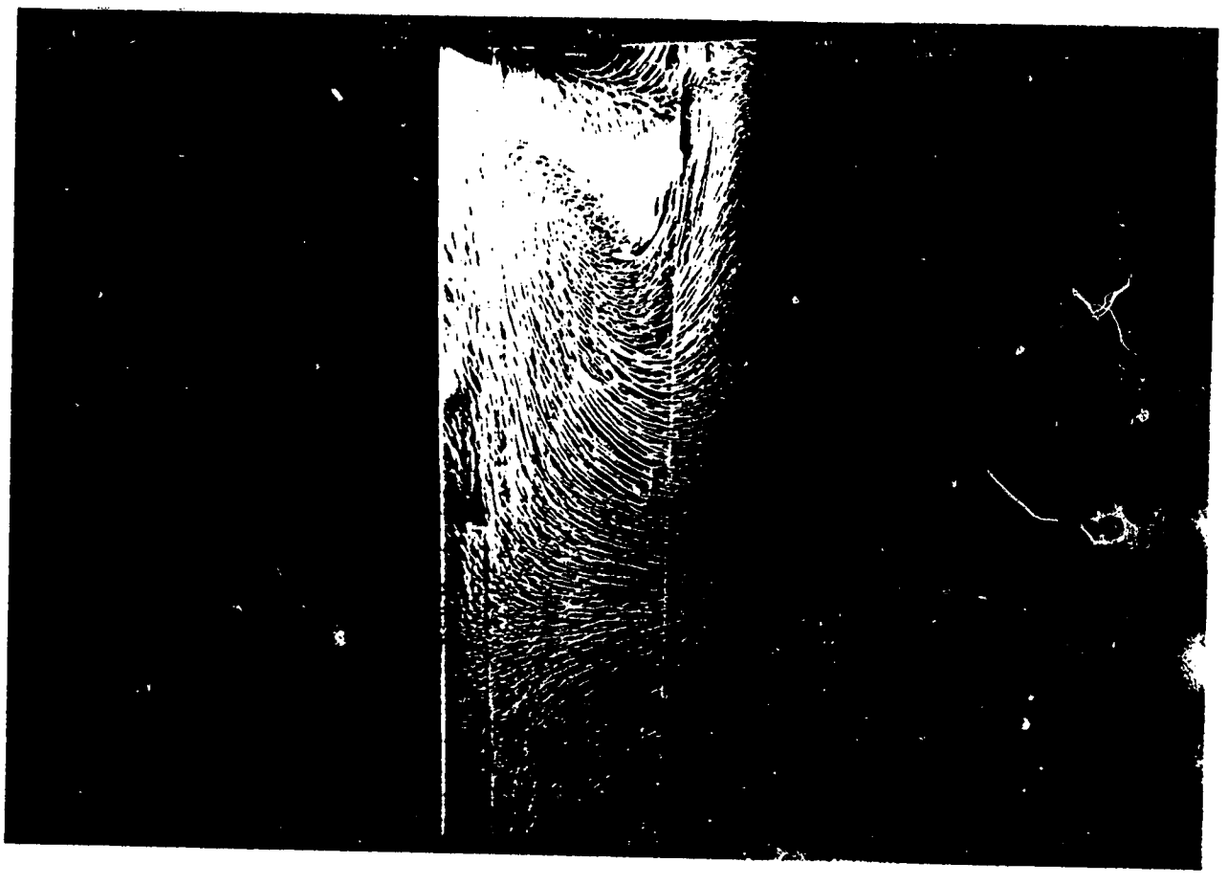

Fig. 19 - Flow Pattern
NACA-64_1A211, Conf. - $N_1 = N_2 = N_3 = 0^o$
$V = 67.06$ m/s, $\alpha = 30^o$

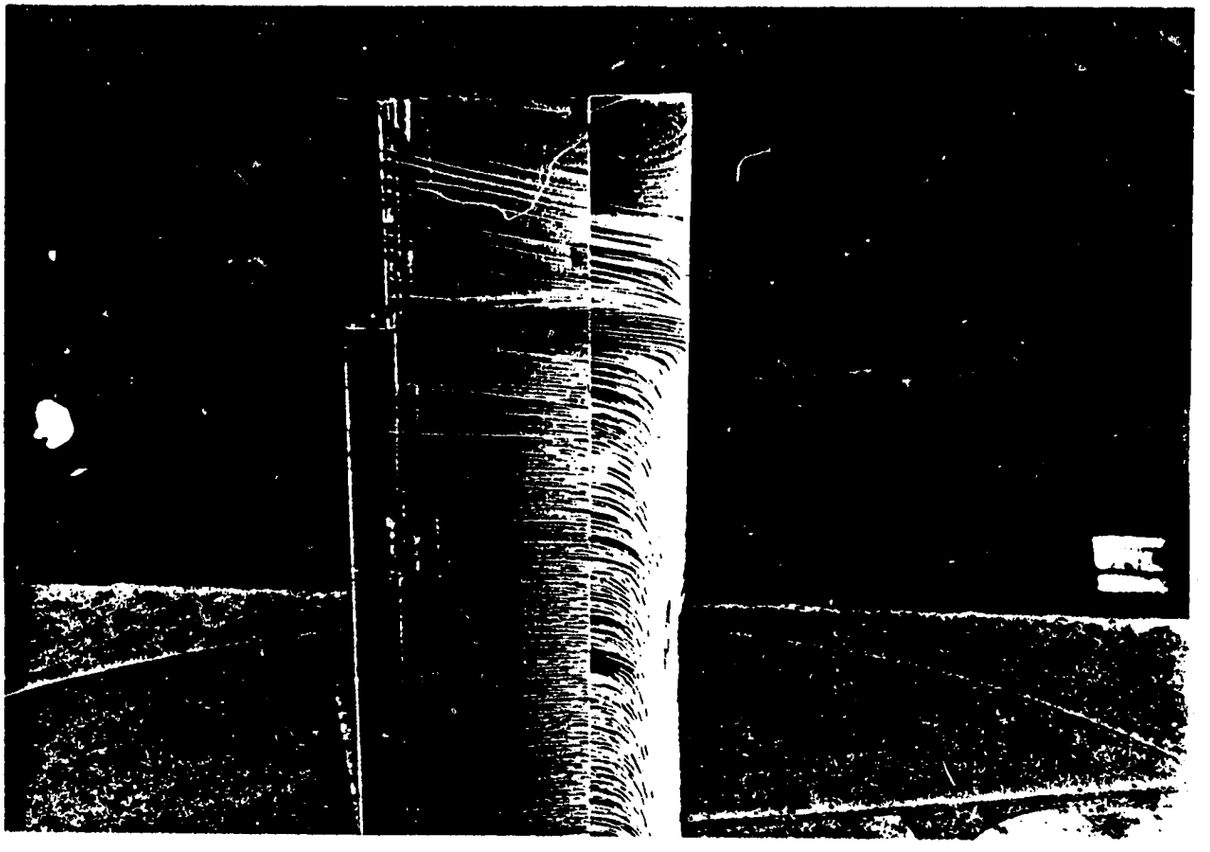

Fig. 20 - Flow Pattern
NACA-64$_1$A211, Conf. - $N_1 = N_2 = 0^o$ $N_3 = 20^o$
V = 67.06 m/s, $\alpha = 15^o$

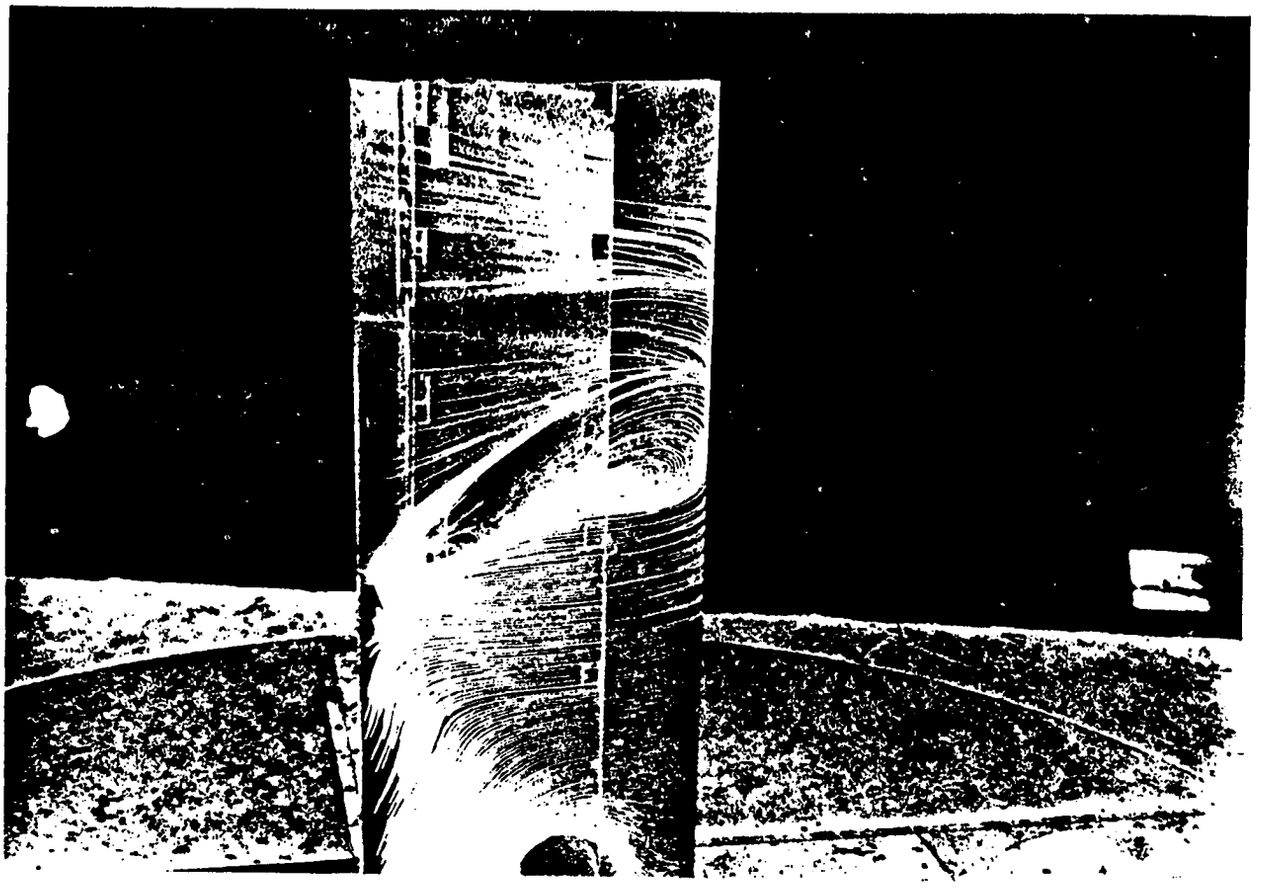

Fig. 21 - Flow Pattern
NACA-64_1A211, Conf. - $N_1 = N_2 = 0^o$, $N_3 = 20^o$
V = 67.06 m/s, $\alpha = 16^o$

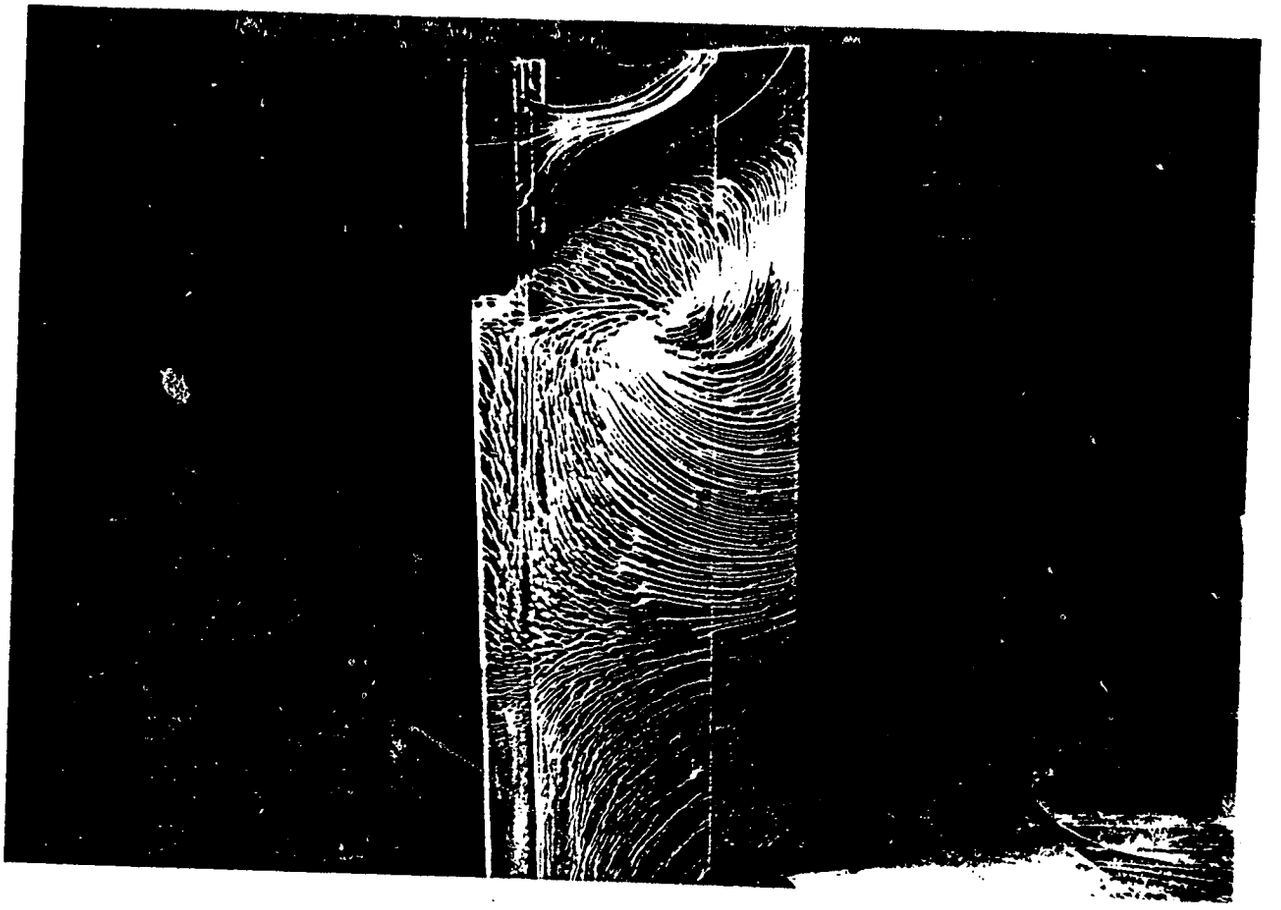

Fig. 22 - Flow Pattern
NACA-64$_1$A211, Conf. - $N_1 = N_2 = 0^o$, $N_3 = 20^o$
V = 67.06 m/s, $\alpha = 30^o$

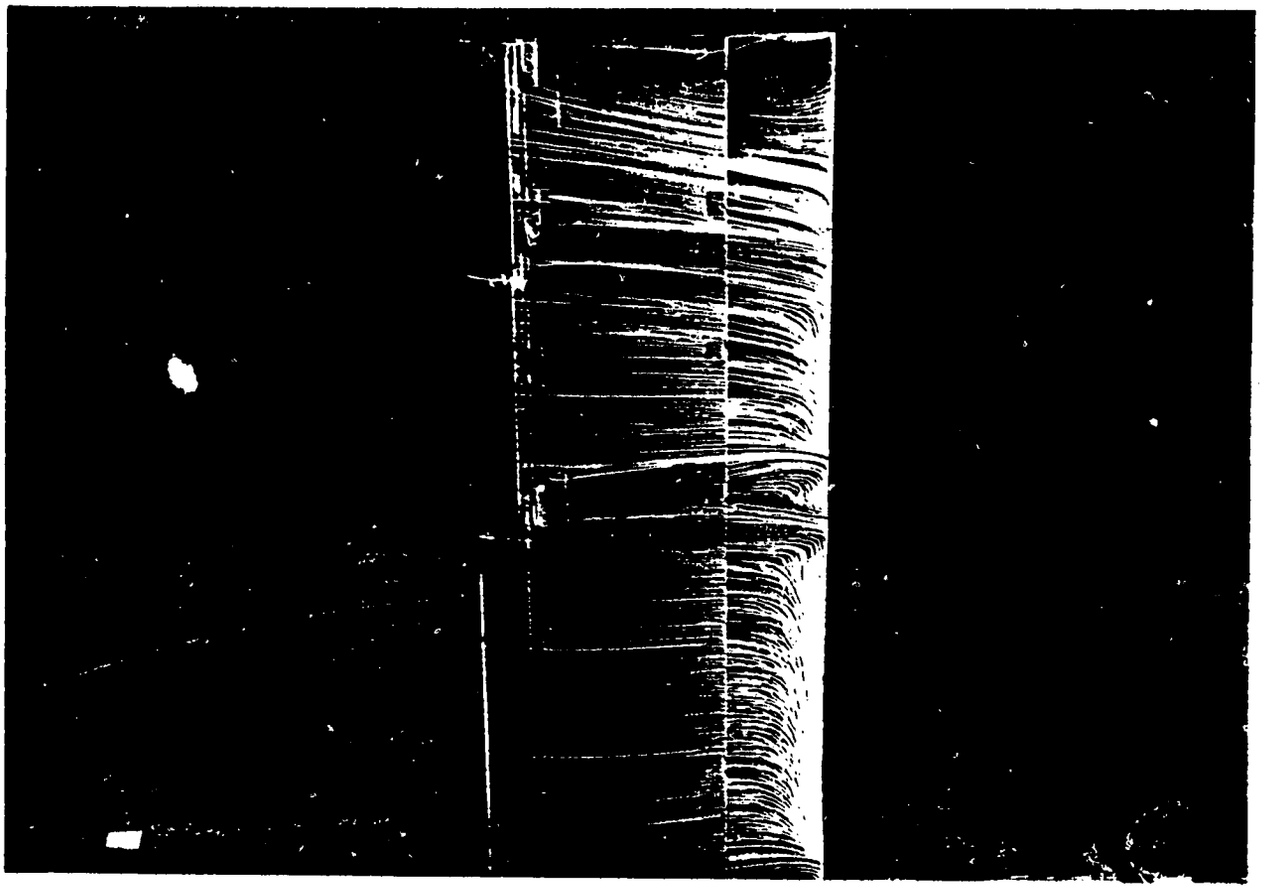

Fig. 23 - Flow Pattern
NACA-64$_1$A211, Conf. - $N_1 = 0^o$, $N_2 = N_3 = 20^o$
$V = 67.06$ m/s, $\alpha = 14^o$

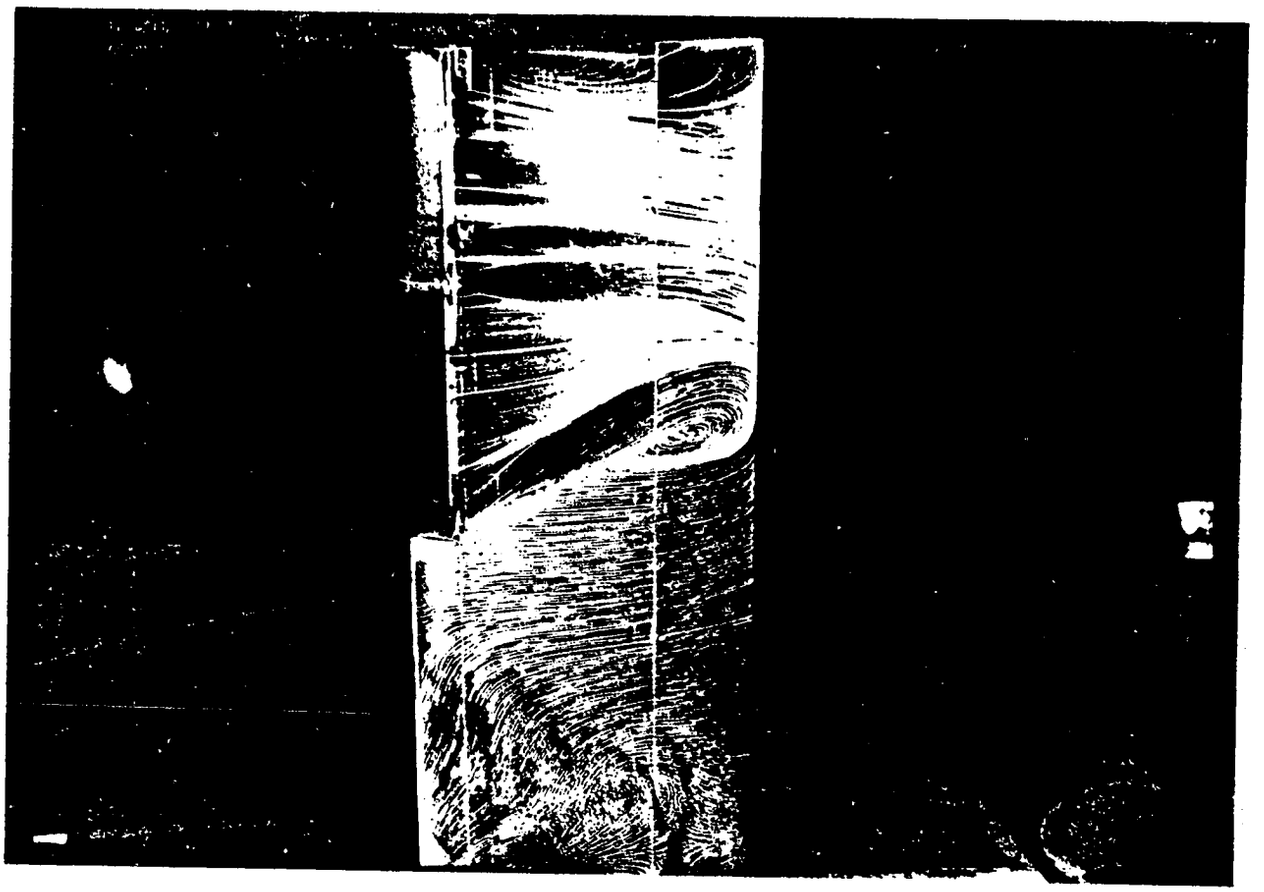

Fig. 24 - Flow Pattern
NACA-64$_1$A211, Conf. - $N_1 = 0^o$, $N_2 = N_3 = 20^o$
V = 67.06 m/s, $\alpha = 16^o$

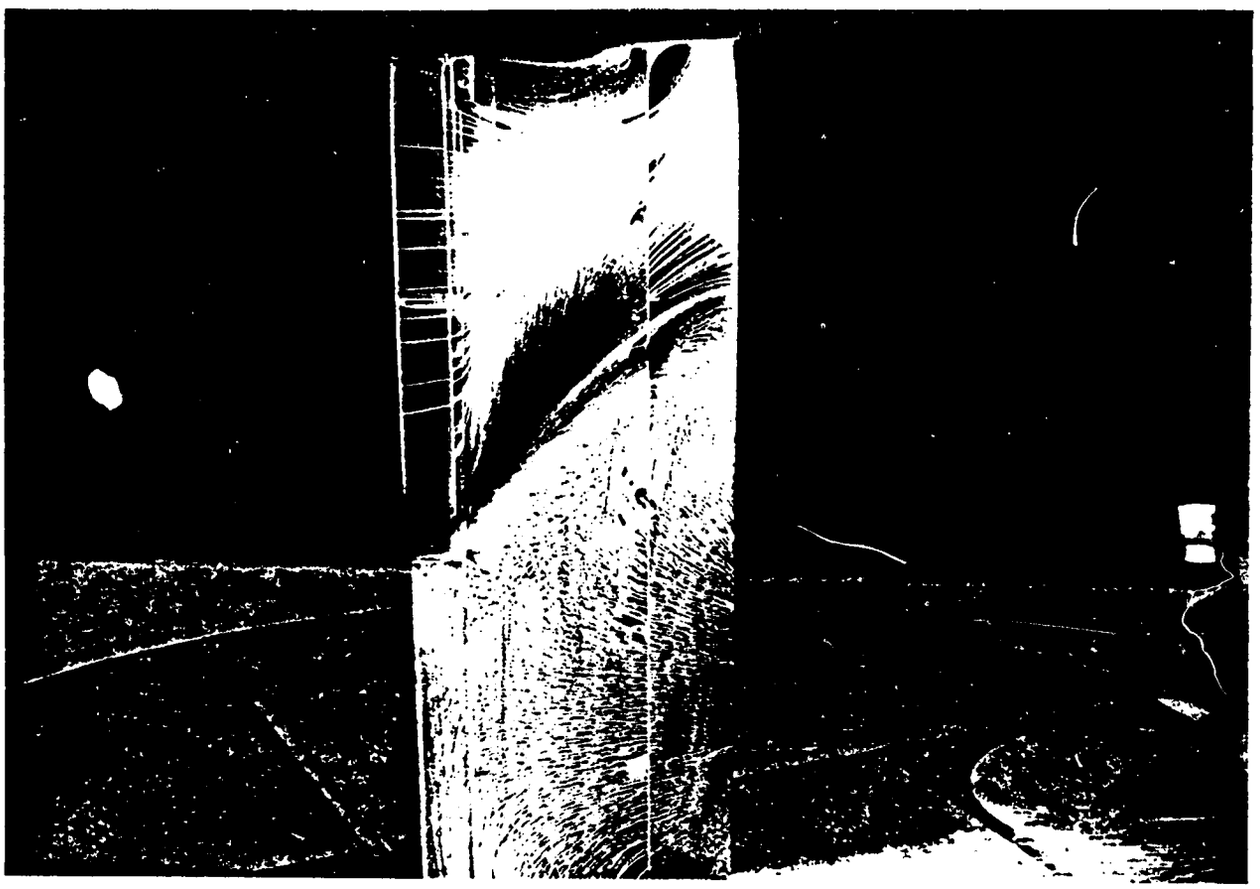

Fig. 25 - Flow Pattern
NACA-64_1A211. Conf. : $N_1 = 0^o$, $N_2 = N_3 = 20^o$
V = 67.06 m/s, $\alpha = 30^o$

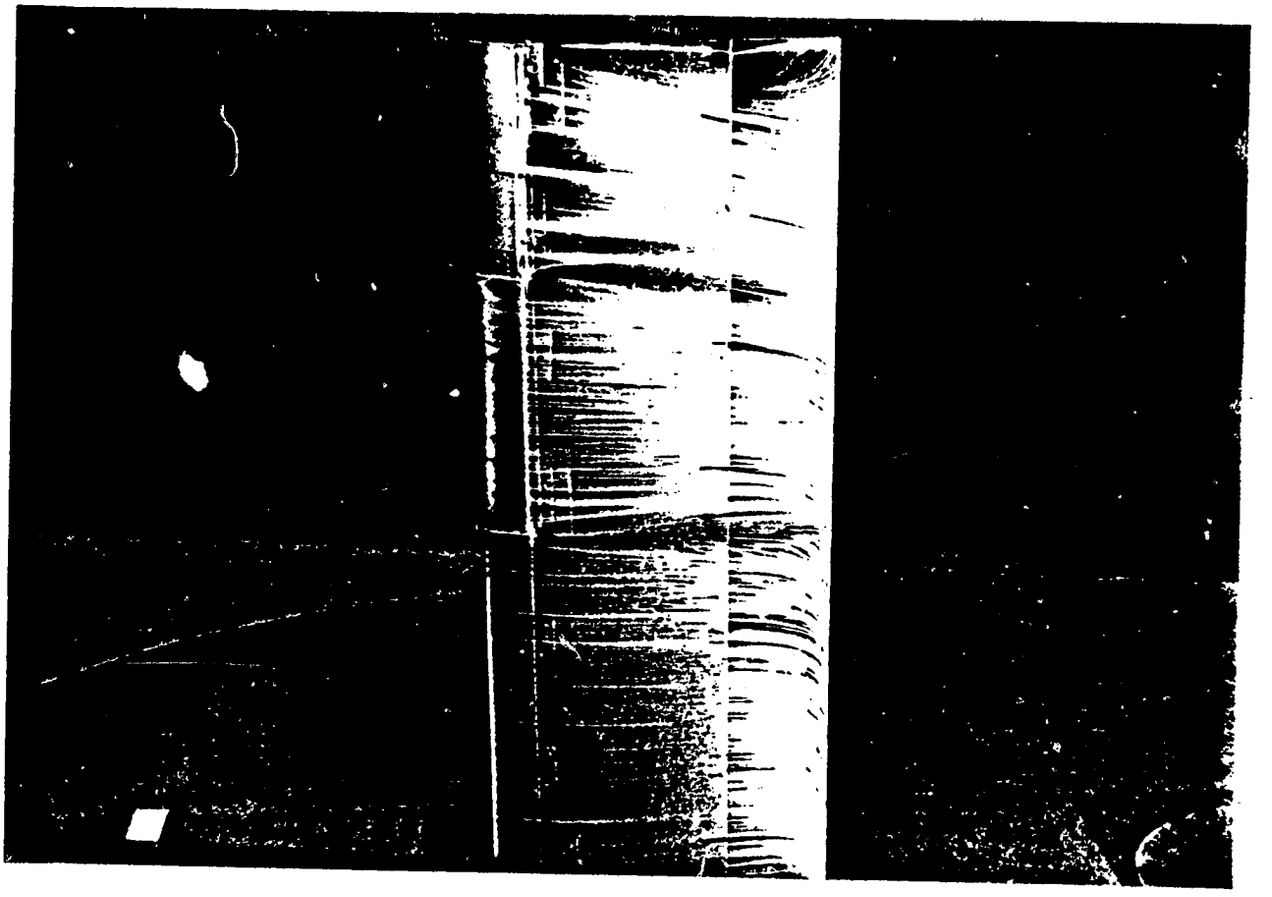

Fig. 26 - Flow Pattern
NACA-64_1A211, Conf. - $N_1 = 0^o$, $N_2 = 10^o$,
$N_3 = 20^o$
V = 67.06 m/s, $\alpha = 10^o$

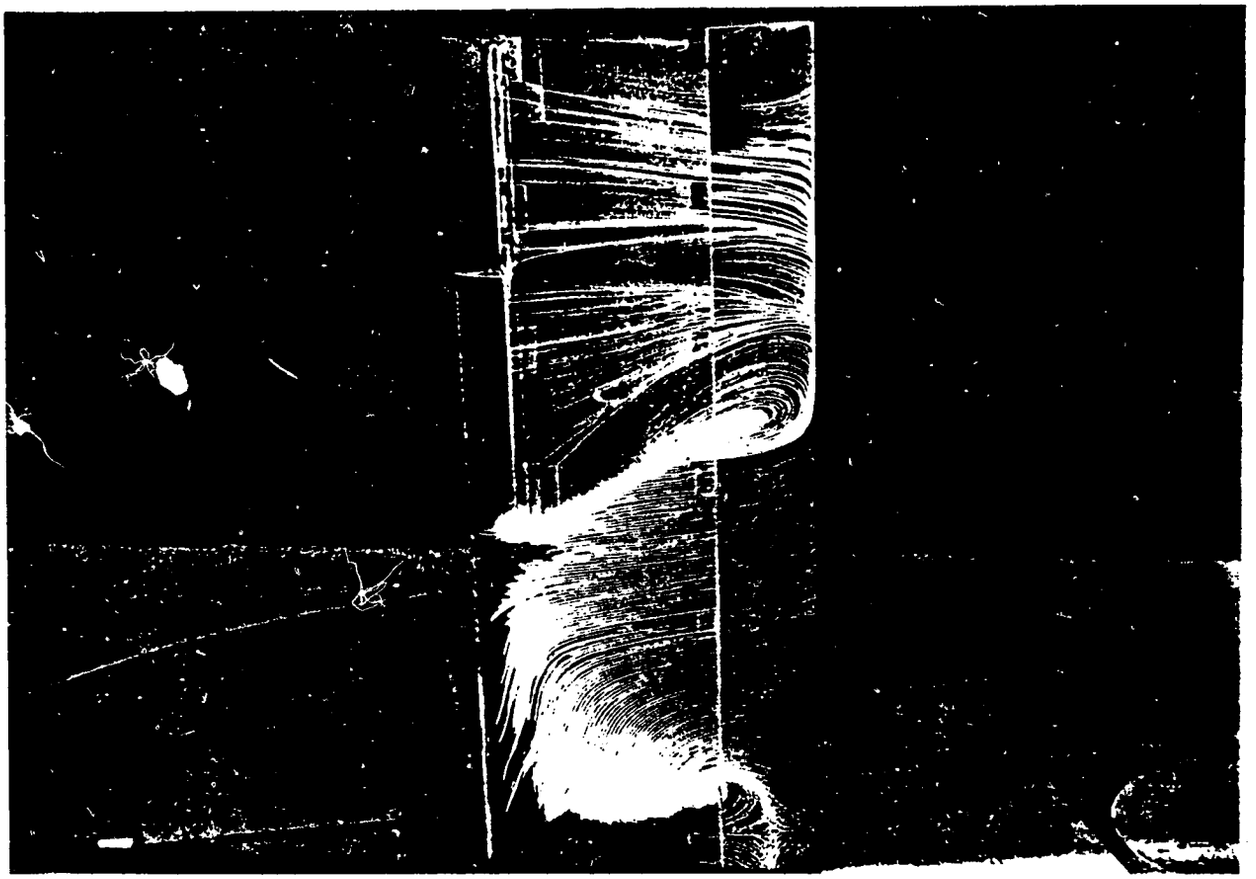

Fig. 27 - Flow Pattern
NACA-64$_1$A211, Conf. -- $N_1 = 0^o$, $N_2 = 10^o$,
$N_3 = 20^o$
V = 67.06 m/s, $\alpha = 16^o$

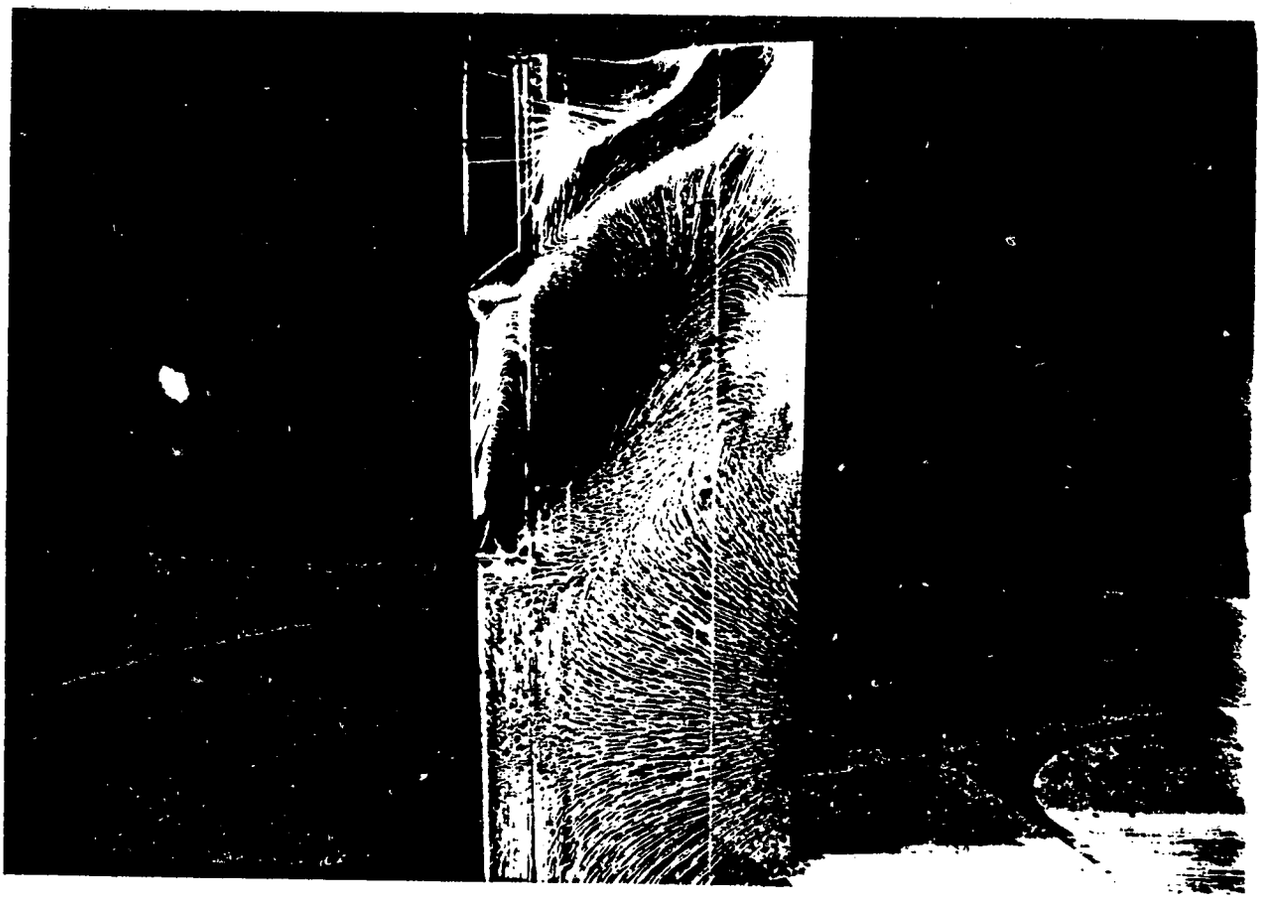

Fig. 28 - Flow Pattern .
NACA-64_1A211, Conf. - $N_1 = 0^o$, $N_2 = 10^o$,
$N_3 = 20^o$
$V = 67.06$ m/s, $\alpha = 30^o$

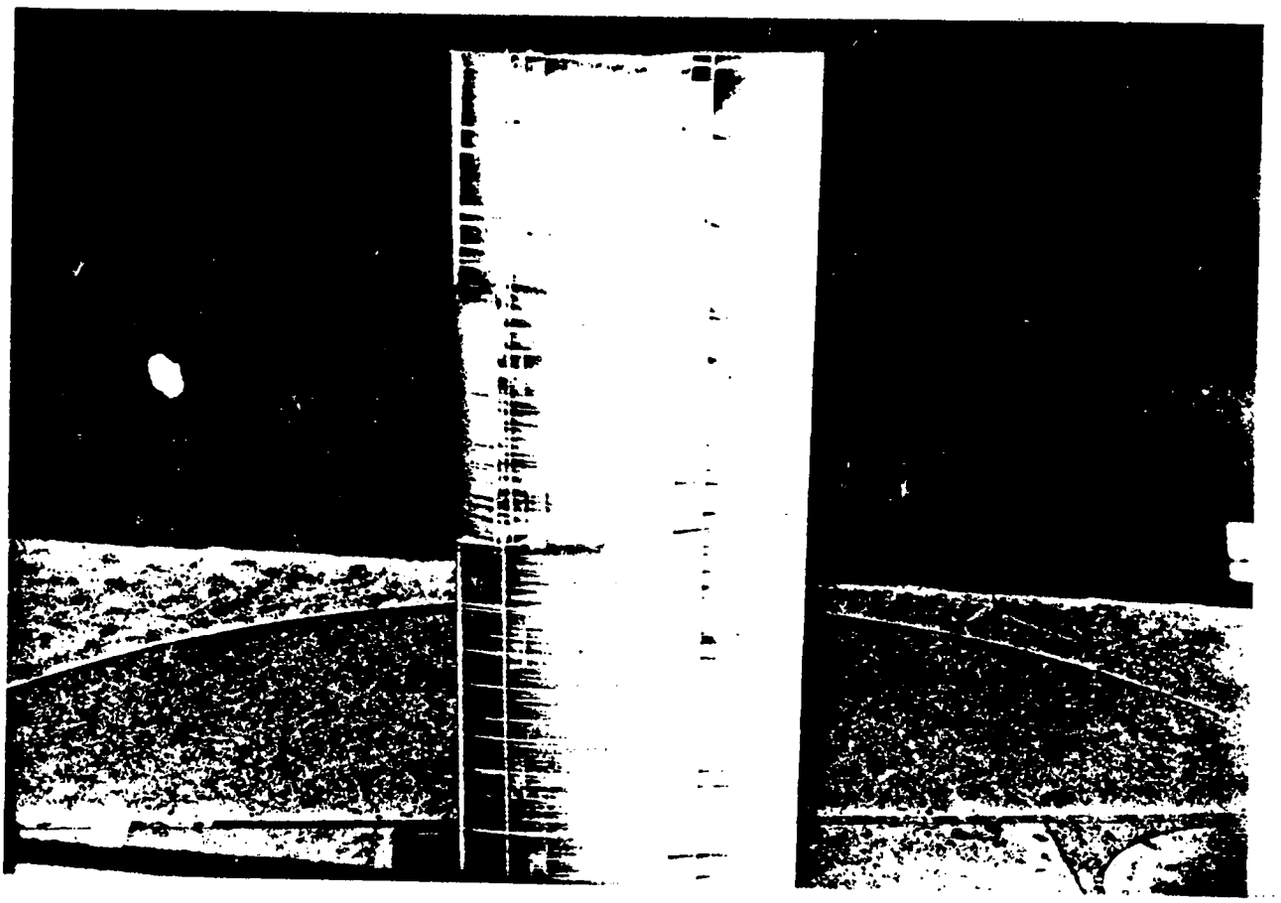

Fig. 29 - Flow Pattern
NACA-64_1A211, Conf. - $N_1 = 0^o$, $N_2 = 20^o$,
$N_3 = 0^o$
$V = 67.06$ m/s, $\alpha = 10^o$

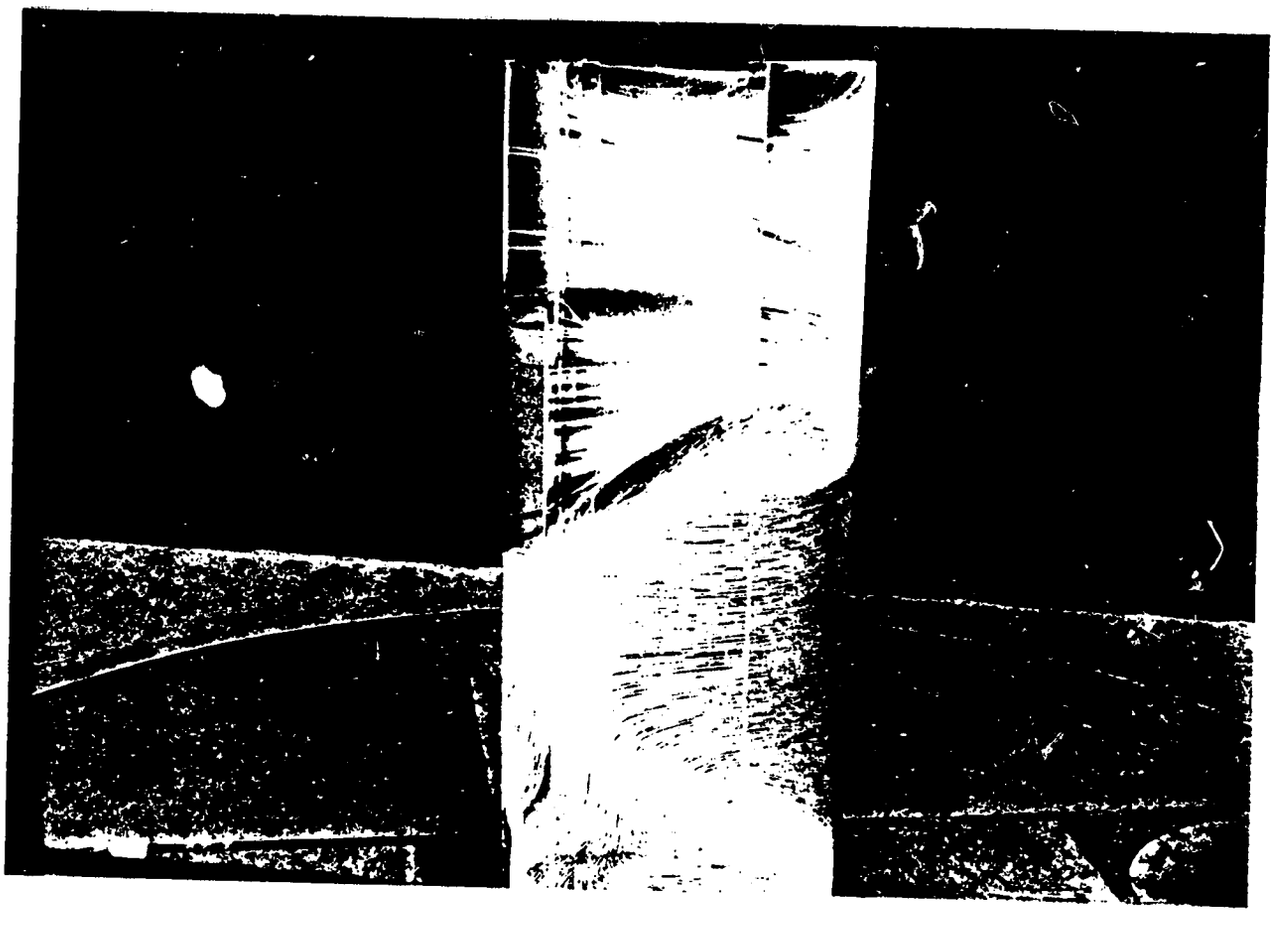

Fig. 30 - Flow Pattern -
NACA-64_1A211, Conf. - $N_1 = 0^o$, $N_2 = 20^o$,
$N_3 = 0^o$
V = 67.06 m/s, $\alpha = 16^o$

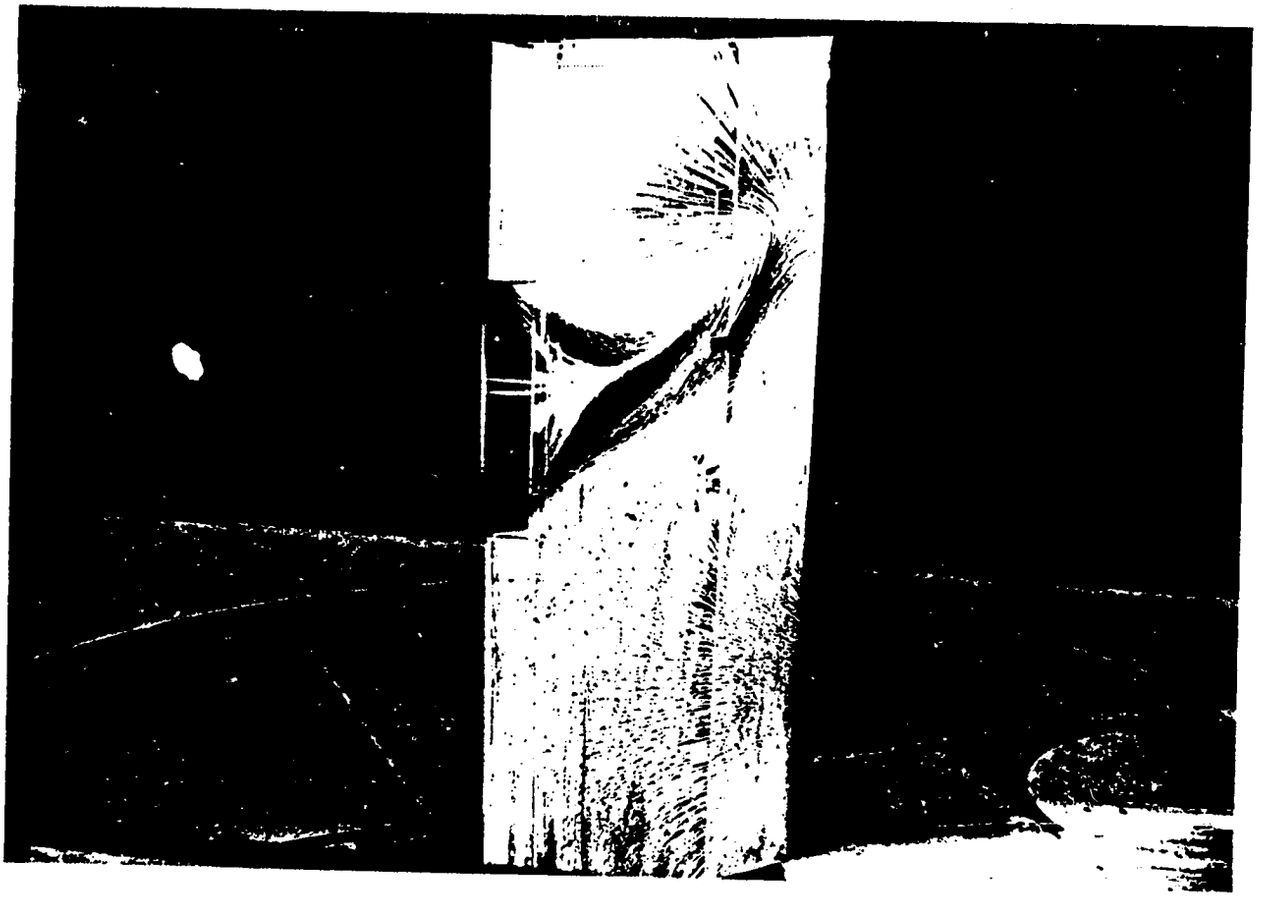

Fig. 31 - Flow Pattern
$NACA\text{-}64_1A211$, Conf. - $N_1 = 0$, $N_2 = 20^\circ$,
$N_3 = 0^\circ$
$V = 67.06$ m/s, $\alpha = 30^\circ$

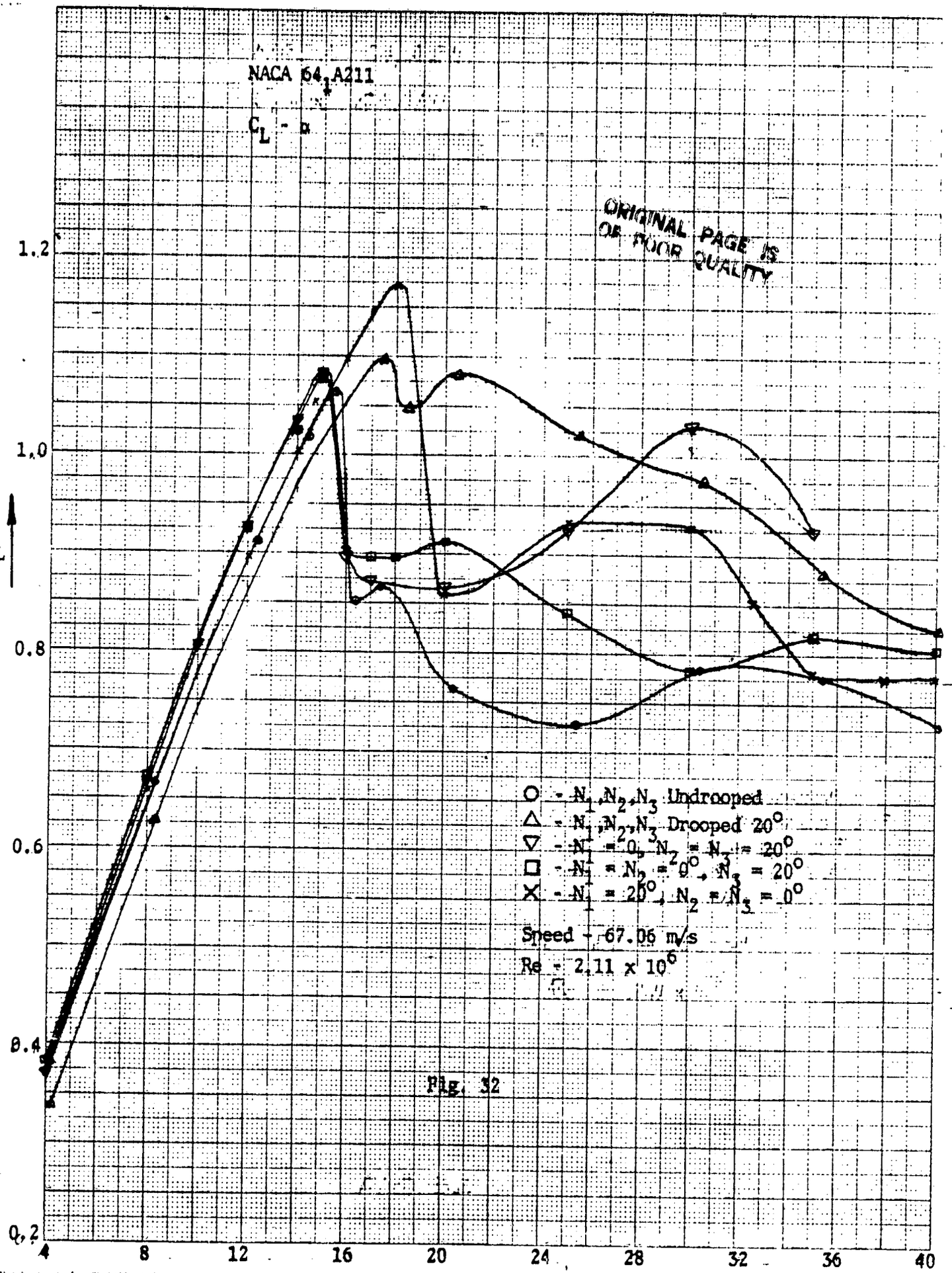

Fig. 32

10 Millimeters to the Centimeter

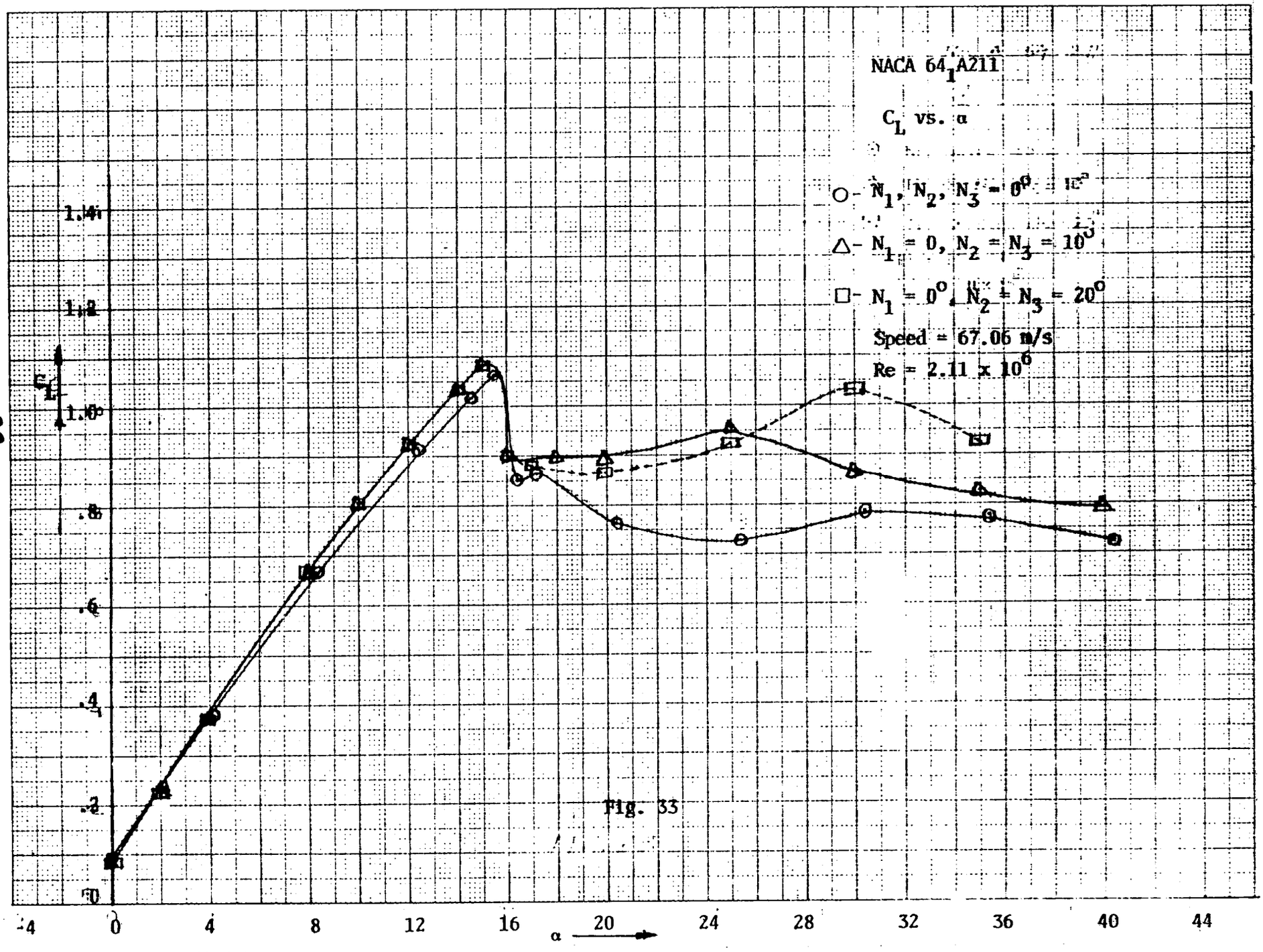

Fig. 33

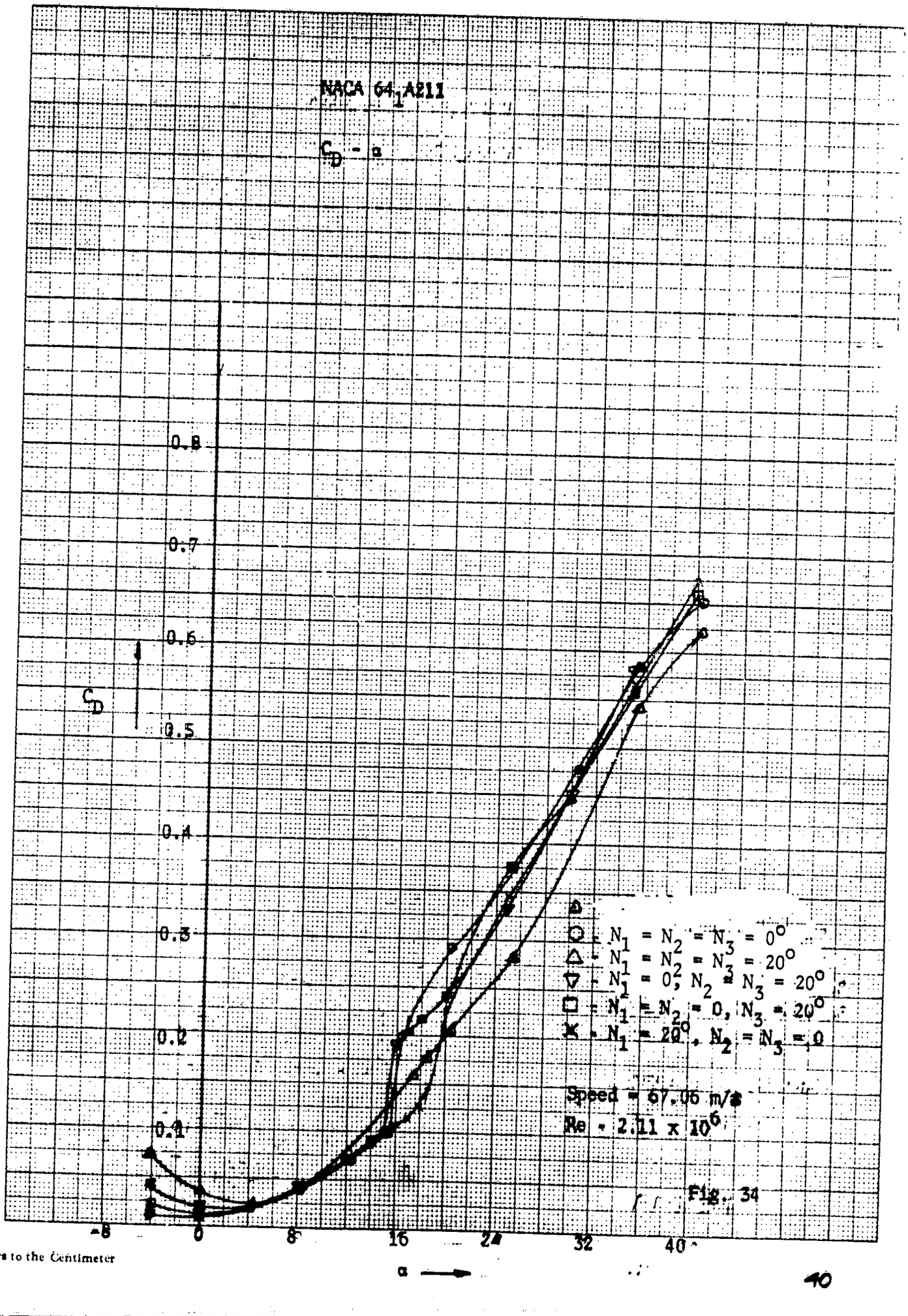

Fig. 34

10 Millimeters to the Centimeter